Title

A microtubule stabilizer ameliorates protein pathogenesis and neurodegeneration in mouse models of repetitive traumatic brain injury.

Journal

Science Translational Medicine, 15(713)

Authors

Zhao, Xinyi

Zeng, Wen

Xu, Hong

et al.

Publication Date

2023-09-13

DOI

10.1126/scitranslmed.abo6889

Peer reviewed

HHS Public Access

Author manuscript

Sci Transl Med. Author manuscript; available in PMC 2024 January 13.

Published in final edited form as:

Sci Transl Med. 2023 September 13; 15(713): eabo6889. doi:10.1126/scitranslmed.abo6889.

A microtubule stabilizer ameliorates protein pathogenesis and neurodegeneration in mouse models of repetitive traumatic brain injury

Xinyi Zhao[1,2,†], **Wen Zeng**[1,2,†], **Hong Xu**[3,†], **Zihan Sun**[1,2], **Yingxin Hu**[1,2], **Beibei Peng**[1], **Jennifer D. McBride**[3], **Jiangtao Duan**[1], **Juan Deng**[1], **Bin Zhang**[3], **Soo-Jung Kim**[3], **Bryan Zoll**[3], **Takashi Saito**[4,5], **Hiroki Sasaguri**[4], **Takaomi C. Saido**[4], **Carlo Ballatore**[6], **Haishan Yao**[7], **Zhaoyin Wang**[1,2], **John Q. Trojanowski**[3], **Kurt R. Brunden**[3], **Virginia M.-Y. Lee**[3,*], **Zhuohao He**[1,2,7,*]

[1]Interdisciplinary Research Center on Biology and Chemistry, Shanghai Institute of Organic Chemistry, Chinese Academy of Sciences, Shanghai 201210, China.

[2]University of the Chinese Academy of Sciences, Beijing 100049, China.

[3]Department of Pathology and Laboratory Medicine, Institute on Aging and Center for Neurodegenerative Disease Research, University of Pennsylvania School of Medicine, Philadelphia, PA 19104, USA.

[4]Laboratory of Proteolytic Neuroscience, RIKEN Center for Brain Science, Wako, Saitama 351-0198, Japan.

[5]Department of Neurocognitive Science, Institute of Brain Science, Nagoya City University Graduate School of Medical Science, Nagoya, Aichi 467-8601, Japan.

[6]Skaggs School of Pharmacy and Pharmaceutical Sciences, University of California, San Diego, La Jolla, CA 92093, USA.

[7]Center for Excellence in Brain Science and Intelligence Technology, Chinese Academy of Sciences, Shanghai 200031, China.

Abstract

Tau pathogenesis is a hallmark of many neurodegenerative diseases, including Alzheimer's disease (AD). Although the events leading to initial tau misfolding and subsequent tau spreading in patient brains are largely unknown, traumatic brain injury (TBI) may be a risk factor for tau-mediated neurodegeneration. Using a repetitive TBI (rTBI) paradigm, we report that rTBI induced

*Corresponding author. hezh@sioc.ac.cn (Z.H.); vmylee@upenn.edu (V.M.-Y.L.).
†These authors contributed equally to this work.

Author contributions: Z.H. conceived and, along with V.M.-Y.L., supervised the project. Z.H. developed the TBI system. Z.H., X.Z., W.Z., and H.X. performed major experiments and analyzed the data. Z.S., Y.H., J.D.M., B.P., and J. Deng were involved in CNDR51657 and mTauKO studies. B. Zoll was involved in data related to PS19 mice. B. Zhang and S.-J.K. conducted mouse stereotaxic injection. J.D.M., S.-J.K., and J. Duan maintained the mouse lines. T.S., H.S., and T.C.S. provided the APP-KI (NL-F) mouse line. C.B., H.Y., Z.W., K.R.B., and J.Q.T. contributed valuable resources and suggestions. Z.H., K.R.B., and V.M.-Y.L. wrote the manuscript with the help from X.Z., W.Z., and H.X. All other authors revised the manuscript.

Competing interests: C.B., K.R.B., V.M.-Y.L., and J.Q.T. are inventors on U.S. patent 9,649,317 "Heterocyclic compounds and their use for the treatment of neurodegenerative disease" that has claims directed to CNDR51657. K.R.B. is a scientific advisory board member for Pinteon Inc., which has provided no funding or advice on the current studies.

somatic accumulation of phosphorylated and misfolded tau, as well as neurodegeneration across multiple brain areas in 7-month-old tau transgenic PS19 mice but not wild-type (WT) mice. rTBI accelerated somatic tau pathology in younger PS19 mice and WT mice only after inoculation with tau preformed fibrils and AD brain–derived pathological tau (AD-tau), respectively, suggesting that tau seeds are needed for rTBI-induced somatic tau pathology. rTBI further disrupted axonal microtubules and induced punctate tau and TAR DNA binding protein 43 (TDP-43) pathology in the optic tracts of WT mice. These changes in the optic tract were associated with a decline of visual function. Treatment with a brain-penetrant microtubule-stabilizing molecule reduced rTBI-induced tau, TDP-43 pathogenesis, and neurodegeneration in the optic tract as well as visual dysfunction. Treatment with the microtubule stabilizer also alleviated rTBI-induced tau pathology in the cortices of AD-tau–inoculated WT mice. These results indicate that rTBI facilitates abnormal microtubule organization, pathological tau formation, and neurodegeneration and suggest microtubule stabilization as a potential therapeutic avenue for TBI-induced neurodegeneration.

INTRODUCTION

Tau is a microtubule-binding protein, enriched in axons, where it serves important roles in microtubule structure and function as well as axonal transport. The pathological transformation of tau is a common feature of a group of neurodegenerative diseases collectively called tauopathies (1, 2), including Alzheimer's disease (AD), frontotemporal lobar degeneration (FTLD), and chronic traumatic encephalopathy (CTE) (3, 4). The structure of tau filaments differs between neurodegenerative diseases, indicating that there could be different tau strains (5). The distribution and burden of distinct pathological tau strains correlates well with clinical brain dysfunction in diverse tauopathy patients (6–10), suggesting that tau pathogenesis plays a key role in the progression of neurodegeneration (4, 11). However, it remains largely unclear what causes or promotes tau pathogenesis in tauopathies.

Poorly defined cellular events lead to monomeric tau misfolding and assembly to multimeric structures that can recruit tau and undergo elongation into the fibrils. Recent data suggest that multimeric tau assemblies can also be released extracellularly to initiate cycles of seeded tau pathology that appear to spread along connected neural networks within the patients' brain over time in a self-propagating manner (12–19).

An important question is what causes initial tau seed formation. Because most tauopathies are sporadic (20), nonautosomal dominant risk factors presumably play a role in tau pathogenesis. CTE frequently occurs in people who experienced repetitive traumatic brain injuries (rTBIs) and shares similarities in histopathology with AD and FTLD, including tau inclusions, as well as accumulation of TAR DNA binding protein 43 (TDP-43). In this regard, football players or boxers have an increased incidence of CTE (2, 21–23). Here, we investigate how repeated brain injury could contribute to the development of tau pathology and neurodegeneration using a modified rTBI paradigm in several tauopathy-related mouse models.

RESULTS

Characterization of the rTBI paradigm in 7-month-old PS19 mice

To examine the relationship between rTBI and tau pathogenesis, we started with the widely used PS19 tauopathy mouse model on a B6C3 mixed genetic background (24). This mouse line overexpresses the human 1N4R tau isoform harboring the familial FTLD-associated $Pro^{301}Ser$ mutation driven by the mouse prion protein (mPrnp) promoter. Immunohistochemical staining with $pSer^{202}/pThr^{205}$ phospho-tau (pTau) antibody AT8 showed that PS19 mice developed visible pathological tau accumulation in the hippocampus starting at 9 to 12 months of age (fig. S1, A to O). We used a brain impact paradigm modified from previous reports (25–27). We performed two repeated impacts onto the midpoints between bregma and lambda along the sagittal suture of the skulls of immobilized 7-month-old PS19 mice using an electromagnetically driven, silicone-tipped metal probe. The interval between the two impacts was 24 hours (fig. S2, A and B). Relative to sham-treated PS19 mice, mice receiving rTBI showed an increase in activated microglia, indicated by an increase in Iba-1 (ionized calcium-binding adapter molecule 1)–positive cells with enlarged cell bodies and thicker processes (Fig. 1A). At 3 days post-rTBI treatment (d.p.t.), the number of Iba-1–positive cells was increased in the cortex, the corpus callosum (Cc), the hippocampus, and the optic tract, a region that is away from the direct impact sites. At 7 d.p.t., the number of Iba-1–positive cells was normalized in Cc, cortex, and hippocampus but still increased in the optic tract at 7 d.p.t. (Fig. 1A). Reactive astrocytes, another marker of neuroinflammation, were examined by glial fibrillary acidic protein (GFAP) staining. GFAP-positive astrocytes were present in the cortex, Cc, hippocampus, and optic tract (fig. S2C). Immunohistochemical staining with anti-phosphorylated neurofilament heavy/medium chain (pNFH/M) antibody TA51 revealed pNFH/M accumulations in neuronal cell bodies and processes in the cortices of rTBI-treated PS19 mice 3 and 7 d.p.t. Moreover, spheroid-like accumulations of pNFH/M were also detected in processes from the hippocampal regions and optic tracts of rTBI-treated, but not sham-treated, mice (Fig. 1B), suggesting that the rTBI paradigm induced neuronal and axonal damage (28). Using the monoclonal antibody 22C11, we further detected accumulations of the amyloid precursor protein (APP) in axon-enriched regions such as the Cc at 3 and 7 d.p.t. (Fig. 1, C and D). These data reveal that the rTBI paradigm used recapitulates certain features of rTBI observed in the human brain, including glial activation as well as neuronal and axonal impairments. These effects occurred not only in the cortex region adjacent to the impact site but also in more distant regions, including the Cc, hippocampus, and optic tract, suggesting widespread diffuse damages.

rTBI increases tau pathogenesis in older male PS19 mice

To examine whether tau pathogenesis is affected by rTBI, we performed rTBI on PS19 mice at 3 months of age, when endogenous tau pathology has not yet developed. The extent of tau pathology was assessed by immunohistochemistry with the AT8 antibody at 1 week and 1, 3, and 6 months post-rTBI treatment (m.p.t.). We only observed a trend toward increased hippocampal tau pathology at 3 m.p.t. (Fig. 2, A and B, and fig. S3A), and we did not examine time points beyond 6 m.p.t. to minimize the confounding effect of endogenous tau accumulation in the older PS19 mice. Next, we investigated the

consequences of rTBI in 7-month-old PS19 mice beyond the 7 d.p.t. previously investigated (Fig. 1). Because untreated 7-month-old PS19 mice started to show some AT8 staining in the superficial cortical layers but hippocampal AT8 staining was largely absent until 12 months of age, we focused on the hippocampal regions to distinguish rTBI-induced tau pathology from endogenous tau pathogenesis. We detected increases in AT8-positive neurofibrillary tangle (NFT)– and neuropil thread (NT)–like pathology at 1 and 3 m.p.t. in rTBI-treated as compared with sham-treated PS19 mice (Fig. 3, A and B, and fig. S3B), suggesting that the facilitation in AT8-positive NFTs/NTs was related to rTBI treatment. To further confirm that rTBI promotes tau pathology, we conducted immunohistochemistry with the MC1 antibody, which binds to misfolded pathological tau. Increased MC1-positive misfolded tau pathology was detected in the hippocampal regions of rTBI-PS19 (7 months) mice compared with sham-PS19 (7 months) mice (Fig. 3, C and D). We did not investigate time points beyond 3 m.p.t. to minimize the confounding effect of endogenous tau accumulation in the older PS19 mice (fig. S1, A to O).

rTBI treatment did not induce tau pathology in similar-aged (8 months) female PS19 mice (fig. S4A), and further examination showed that aged female PS19 mice express much fewer tau proteins than male mice do (fig. S4B), consistent with other reports (29–32). rTBI treatment did not induce NFT-like tau pathology in 8-monthold wild-type (WT) mice (fig. S5, A to D), indicating that aging alone was not sufficient to develop NFT-like tau pathology after rTBI.

To further explore why rTBI increased tau pathogenesis in older but not younger PS19 male mice, we examined endogenous pathological tau accumulation in male PS19 mice of different ages. Whereas immunohistochemical staining using AT8 antibody showed almost no detectable NFT-like pathological tau in the hippocampal regions of PS19 mice before 10 months of age (fig. S1, A to O), sequential biochemical extraction of hippocampi from PS19 mice at different ages to obtain sarkosyl-insoluble protein showed that pTau (PHF-1, $pSer^{396}/pSer^{404}$) could be detectable in PS19 mouse brains as early as 6 months of age (Fig. 3, E and F).

rTBI accelerates tau pathogenesis in young PS19 mice inoculated with tau PFFs

The observation that tau pathogenesis was increased by rTBI at 7 but not 3 months of age in male PS19 mice, and that insoluble pathological tau accumulation could not be detected until 6 months of age, led us to hypothesize that accumulating pathological tau in 7-month-old PS19 mice may function as endogenous seeds and that rTBI treatment could facilitate the seeding process. If true, then supplying exogenous tau seeds in younger PS19 mice should lead to an rTBI-triggered increase of tau pathology similar to that seen in older PS19 mice. To test this hypothesis, we used a previously developed pathological tau seeding model in which intracerebral injection of tau preformed fibrils (PFFs) made from recombinant tau protein into young PS19 mice induces tau pathological inclusions within a short time (12). We first injected tau PFFs into the right dorsal hippocampi of 3-month-old female PS19 mice (PFF-PS19). A week later, the mice received rTBI or sham treatments, and the extent of tau pathology was examined at different time points (fig. S6A). An acceleration of AT8-positive tau pathology was observed in rTBI-treated PFF-

PS19 mice compared with sham-treated PFFPS19 mice at 1 week post-treatment (w.p.t.) in the ipsilateral hemisphere (Fig. 4, A and B). No AT8 staining was observed in phosphate-buffered saline (PBS)–injected PS19 mice after sham or rTBI treatment at 1 w.p.t. (Fig. 4, A and B). Staining with the tau conformation–selective MC1 antibody showed a similar trend (Fig. 4C and fig. S6B). Moreover, mapping of MC1 immunohistochemistry-derived tau pathology scores (see Materials and Methods) illustrated that seeded tau pathology affected more brain regions in rTBI-treated PFF-PS19 mice in comparison with sham controls (Fig. 4D and fig. S7A). The pathology scores in rTBI-PFF-PS19 mice were substantially higher in brain regions such as the subiculum (ipsilateral: $P = 0.007$; contralateral: $P = 0.022$; fig. S7, B and C), ventral hippocampal hilus (ipsilateral: $P = 0.103$; contralateral: $P = 0.027$; fig. S7, D and E), and entorhinal cortex (ipsilateral: $P = 0.004$; contralateral: $P = 0.052$; fig. S7, F and G).

rTBI facilitates tau pathology in WT mice inoculated with AD brain–derived pathological tau

To eliminate any influence of transgene expression in the PS19 line, we next used a previously described tau transmission model in female WT mice, where intracerebral injection of brain-derived pathological tau from patients with AD induces AD-like tau inclusions that are composed of endogenous murine tau at 3 months post-injection (m.p.i.) (13, 15, 16). We extracted tau from frontal cortical tissues of four donors with a primary neuropathological diagnosis of AD and one donor with no detectable protein pathologies (Fig. 5A, fig. S8, and table S1). AD-tau isolated from patient 1 (AD1-tau) was injected into the right dorsal hippocampal and overlying cortical regions of 3-month-old female WT mice. Aweek later, rTBI or sham treatments were performed, and tau pathology was examined at different time points (fig. S9A). rTBI-treated mice injected with AD1-tau showed reduced thickness and increased AT8-positive NT tau staining in the Cc that was not seen in mice injected with N.C. (normal control) extract (Fig. 5, B and C, and fig. S9B). The amount of AT8-positive staining in the Cc increased over time (Fig. 5C). Immunohistochemical staining with MC1 antibody confirmed the accelerated tau pathology in the Cc of rTBI-treated AD1-WT mice (fig. S9C). Staining with the neuronal axon markers neurofilament light chain (NFL, NFL1/2) or pNFH/M (TA51) revealed no changes in the Cc (fig. S9, D to G). At 3 m.p.t., rTBI-treated AD1-WT mice showed no difference in AT8-positive NFTs in the hippocampus as compared to sham-treated mice (Fig. 5, D and E, and fig. S10A) but a significant increase of AT8-positive NFTs in the ipsilateral entorhinal cortex ($P = 0.021$; Fig. 5, D and F). Similarly, MC1 staining confirmed accelerated tau pathology in the ipsilateral entorhinal cortices but not hippocampi of the rTBI mice at 3 m.p.t. ($P = 0.018$; fig. S10, B and C).

Mapping of tau pathology scores based on AT8-positive staining (see Materials and Methods) showed that tau pathology affected more brain regions in rTBI-treated as compared with sham-treated AD1-WT mice (fig. S11A), including the fimbria (ipsilateral: $P < 0.001$; contralateral: $P < 0.001$; fig. S11, B and C), retrosplenial cortex (ipsilateral: $P = 0.010$; fig. S11, D and E), and subiculum (ipsilateral: $P < 0.001$; fig. S11, F and G). The affected brain regions have neuroanatomical connections to the site of seed injection.

Double immunofluorescence staining revealed colocalization of AT8 staining with Olig2, an oligodendrocyte marker (Fig. 5G). The number of AT8-positive oligodendrocytes in the Cc and fimbria regions was significantly increased in rTBI-treated AD1-WT mice starting 6 m.p.t. ($P = 0.045$; Fig. 5, H and I).

Given the possibility that there is heterogeneity of AD-tau isolated from different sporadic AD cases, we injected two additional AD-tau preparations (AD2 and AD3; Fig. 5A and fig. S8) into the right dorsal hippocampal regions of WT mice and performed rTBI or sham treatment 1 week later. Similar to the AD1-WT, rTBI accelerated neuronal and oligodendrocytic tau pathogenesis in AD2-WT and AD3-WT mice (fig. S12, A to E). Together, these results suggest that rTBI facilitates the formation of pathological tau in WT mice preseeded with human brain–derived pathological tau seeds.

rTBI induces punctate tau accumulation and phosphor-TDP43 in the optic tracts of WT mice

Although we could not detect any classical NFT-like tau pathology in rTBI-treated WT mice without human brain–derived tau seeding (fig. S5), careful inspection revealed AT8-positive tau puncta in the optic tracts of rTBI-treated WT but not sham-treated WT mice (Fig. 6, A and B, and fig. S13A). We also found these punctate tau accumulations after staining with an alternative pTau antibody, AT180 (fig. S13B). Extraction of endogenous tau from optic nerves confirmed an increase of PHF-1–positive tau in the sarkosyl-insoluble fraction of rTBI-treated WT mice (fig. S13C). NT-like tau pathology was not observed in the Cc of the rTBI-treated WT mice (fig. S13D). rTBI-induced endogenous murine tau puncta were also observed in the optic tracts of APP knock-in (33) mice (fig. S14, A and B).

Staining of the optic tracts with the neuronal axon markers NFL (NFL1/2) or pNFH/M (TA51) revealed nerve tissue shrinkage along with an increase of voids in the optic tracts of rTBI-treated WT mice ($P < 0.01$; Fig. 6, C to F, and fig. S15A), suggesting trauma-induced neuronal degeneration. Axonal damage was not detected in the Cc (fig. S15, B to F). Punctate tau accumulation along with tissue degeneration was also observed in the optic tracts of rTBI-treated WT mice that were preseeded with AD-tau (Fig. 6, G to I, and fig. S16, A to C), where shrinkage and reduced neurofilament staining were also seen (Fig. 6, I to K, and fig. S16, D and E).

TDP43 and α-synuclein (α-Syn) are two other protein markers commonly associated with neurodegenerative diseases, and TDP43 pathology is found in CTE (2) and in patients with AD (34), leading us to examine whether rTBI induced TDP-43 inclusions in our models. Immunohistochemical staining with a phospho-TDP43 (p409/410) showed accumulated TDP-43 deposits in the optic tracts from rTBI-treated WT mice at 9 but not 3 m.p.t. (fig. S17, A and B), when there is already punctate tau (Fig. 6B and fig. S13A). This finding was cross-validated with another phospho-TDP43 (p403/404) antibody (fig. S17C). Some of the phosphorylated TDP43 (pTDP43) colocalized with AT8-positive tau (fig. S17D). An increase of pTDP43 ($pSer^{409}/pSer^{410}$) in the optic tract was also found in rTBI-AD1-WT mice after 6 m.p.t. (fig. S17, E and F), the appearance of which was later than tau pathology (Fig. 6H and fig. S16A).

We also examined for the presence of α-Syn pathology in the optic tracts from rTBI-treated WT mice at 9 m.p.t. using the phospho–α-Syn ($pSer^{129}$) antibody 81A (fig. S17H) and the Syn506 antibody (fig. S17I) that recognizes misfolded α-Syn. However, inconsistent staining patterns were observed with these two different antibodies, and it is thus unclear whether rTBI induced α-Syn pathology.

Tau ablation mitigates rTBI-induced neurodegeneration

Because rTBI-induced TDP43 pathology appeared later than tau pathology, and there was some colocalization of pTDP43 and pTau aggregates, we asked whether the formation of tau inclusions promoted TDP43 pathogenesis and mediated rTBI-induced neurodegeneration. We performed rTBI on *Mapt* knockout mice (mTauKO), which have no endogenous murine tau and are relatively free of obvious phenotypic changes until advanced age (35, 36). Examination of the optic tracts at 9 m.p.t. revealed that punctate AT8 staining was absent in rTBI-mTauKO mice (fig. S17J) and that pTDP43 aggregates were reduced compared with rTBI-WT mice (fig. S17, K and L). Furthermore, although optic tract thickness was similar in rTBI-treated mTauKO mice compared to rTBI-treated WT mice (fig. S17M), the formation of tissue voids was partially reversed in the rTBI-treated mTauKO mice as evidenced by decreased void density and area (fig. S17, N and O), despite the observation that individual void sizes were similar between WT and mTauKO mice after rTBI (fig. S17P).

rTBI causes axonal microtubule abnormalities

The reduced optic tract thickness with associated tissue voids found in rTBI-treated WT mice suggested a loss of neuronal projections. Because tau is a microtubule-binding protein and is thought to play a role in microtubule structure and function, we examined the integrity of axons and axonal microtubules and tested whether chronic treatment with CNDR51657, a previously described brain-penetrant microtubule-stabilizing compound (37–39), could restore rTBI-induced changes at different time points (Fig. 7A). Transmission electron microscopy (TEM) was conducted on sections of the optic nerves. As early as 3 w.p.t., there was evidence of axonal irregularities and shrinkage in the rTBI-treated but not in the sham-treated WT mice (Fig. 7B). Moreover, counts of microtubules in higher-magnification TEM images (Fig. 7B) revealed that there were significantly fewer microtubules per axonal area in the rTBI- than sham-treated WT mice ($P < 0.001$; Fig. 7C) at 3 w.p.t. when there was still barely detectable tau pathology in the optic tract (Fig. 6B and fig. S13A).

To examine whether microtubule disruption is involved in rTBI-induced endogenous tau pathogenesis in WT mice in vivo, we administered CNDR51657 through intraperitoneal injections at 3 mg/kg to WT mice 30 min after each TBI injury and then twice weekly thereafter for up to 24 weeks. Such treatment rescued TBI-induced microtubule disruption in the optic tracts of WT mice at 3 w.p.t. (Fig. 7, A to C). CNDR51657 treatment also increased neurofilament staining in the optic tracts of rTBI-treated WT mice (Fig. 7, D to F, and fig. S18A). Moreover, CNDR51657 treatment increased optic tract thickness and reduced AT8-positive tau accumulation 3 m.p.t. (Fig. 7, G to I, and fig. S18B). Furthermore, CNDR51657 treatment normalized AT8 staining in the cortex and the number

of AT8-positive oligodendrocytes in the fimbria in WT mice pre-inoculated with AD4-tau (Fig. 5A and figs. S8 and S18, C to G).

Next, we examined whether treatment with the microtubule stabilizer CNDR51657 could mitigate rTBI-induced TDP43 pathologies. We found that 24 weeks of treatment with CNDR51657 in rTBI-WT mice greatly reduced pTDP43 accumulation in the optic tracts (fig. S19, A and B), suggesting that the microtubule abnormality is a primary driver of both TBI-induced tau and TDP43 pathogenesis and, as noted, neuronal damage. Together, these data suggest that rTBI-induced protein pathogenesis and neurodegeneration are associated with microtubule disruption and that a brain-penetrant microtubule-stabilizing agent alleviates such pathogenesis and neurodegeneration in the rTBI model.

Microtubule stabilization shows beneficial effects on brain functions of WT mice after rTBI

To examine the effect of microtubule stabilization on functional recovery after rTBI, we first assessed visual function, because pathogenesis and neurodegeneration were observed in the optic tracts of rTBI-treated WT mice (Figs. 6 and 7). Because a large fraction of retinal ganglion cell axons in mice cross over at the optic chiasm to the other hemisphere (40), light stimulation in one eye activates more neurons in the contralateral than the ipsilateral primary visual cortex (V1). Such differential activation of the two brain hemispheres could be diminished by optic nerve impairment. We found that the density of c-Fos–positive cells in layer 4 of V1 was higher in the contralateral than the ipsilateral sides of sham-treated WT mice. This difference in c-Fos staining between the two hemispheres was abolished in rTBI-treated WT mice but could be rescued by chronic CNDR51657 treatment (Fig. 8, A and B). Fiber photometry calcium imaging in the contralateral dorsal lateral geniculate nucleus (dLGN) that receives direct input from the optic nerve showed reduced light-evoked responses in rTBI-treated WT mice compared with sham-treated WT mice. The visual response in rTBI-treated mice could be rescued by CNDR51657 treatment (Fig. 8, C and D).

Motor functions, as assessed by balance beam test (fig. S20A) and a rotarod test (fig. S20B), were similar in rTBI- and sham-treated animals and not affected by CNDR51657 treatment. Open field test (Fig. 8E), light-dark box test (Fig. 8F), and elevated plus maze (Fig. 8G) indicated abnormal anxiety behaviors in rTBI-treated WT mice. CNDR51657 treatment did not normalize these behaviors. Cognitive function was assessed by Y maze (Fig. 8H) and Barnes maze (Fig. 8I). The results indicate short- and long-term spatial memory deficits in rTBI-treated WT mice that received vehicle as compared with sham-treated mice that received vehicle. CNDR51657 alleviated rTBI-induced memory impairments. Together, these results suggest that the microtubule stabilizer CNDR51657 can alleviate some of the rTBI-induced behavioral abnormalities. However, because many of the behavioral tests used depend on visual function, it is not possible to differentiate whether the corrective effects of CNDR51657 resulted from a restoration of brain regions involved in memory processes or restoration of visual function.

DISCUSSION

Using a modified rTBI paradigm in WT mice and multiple AD mouse models, we have demonstrated that rTBI induces de novo tau pathogenesis and facilitates seeded tau

transmission. Moreover, rTBI induced de novo TDP43 pathogenesis that appeared to be at least partially dependent on the formation of tau pathology. Last, rTBI was found to cause neural tissue degeneration. It appears that rTBI exerts such adverse effects, at least in part, through a disruption of axonal microtubules, because treatment with a small-molecule microtubule-stabilizing compound led to a partial rescue of these rTBI-induced pathologies, neuronal impairment, and dysfunction in the optic tract. This study thus provides a body of experimental data to support the causal effect of rTBI on the development of tau pathologies and suggests a potential therapeutic strategy of using microtubule-stabilizing agents for rTBI-induced neurodegeneration.

On the basis of the data presented here and in previous reports (15, 41), we propose a model (fig. S21) in which TBI causes microtubule disruption and axonal damage, facilitating tau to be more prone to be transformed into pathology, possibly through increasing local free tau concentration because of tau detachment from disrupted microtubules in damaged axons or damaging protein quality control machinery because impaired intracellular vesicle transport. This could promote pathogenic seed formation and the elongation of tau seeds that have been internalized through the process of pathological tau transmission. Thus, repeated TBI acting alone or together with other risk factors, such as aging, could facilitate pathological tau formation. Last, TBI also could induce TDP43 pathogenesis, which may be partially mediated by prior formation of tau pathology.

Given the evidence here of microtubule disruption playing a key role in the formation of TBI-induced pathologies, we reason that compounds that promote microtubule normalization might improve axonal transport, which is critical for many essential intracellular events, including autophagy and lysosome formation (42), and reduce the local accumulation of proteins such as APP, BACE1, and tau (43). Moreover, normalizing microtubule structure may result in increased microtubule binding by tau, thereby lowering the local concentration that could facilitate the formation of tau pathology. Our previous studies reported that administration of CNDR51657 decreased Aβ plaque pathology in 5xFAD mice (39) and tau pathology in PS19 mice (38). Combined with the present results, these findings suggest that improving microtubule structure and function could lead to a diminution of pathogenesis, tissue damage, and functional abnormalities in multiple neurodegenerative diseases, including CTE, AD, and FTLD. We administered the first intraperitoneal dose of CNDR51657 30 min after TBI treatment, indicating that TBI-mediated axonal damage can be corrected after the initial insult. It is notable that in the behavior analyses, CNDR51657 showed some evidence of improving long-term spatial memory tests (Fig. 8I). Because rTBI did not invoke motor deficits as measured by balance beam or rotarod testing (fig. S20, A and B), there was no opportunity to observe a compound-mediated correction in these studies. The rTBI paradigm in this study resulted in a mild-to-moderate TBI injury that was intended to recapitulate the damage observed in most human rTBI cases, and as a result, the behavioral deficits may have been relatively subtle, particularly at 4 to 12 w.p.t. testing time. Thus, the evidence of CNDR51657 causing improvements in some behavioral outcomes is consistent with the data showing attenuation of pathological measures upon compound treatment of rTBI mice. We also acknowledge that the improvements observed in the visual cue-dependent behavior tests may have resulted, in part or whole, from a compound-mediated preservation of visual function in the rTBI mice.

We observed that aging could be an important factor in the development of rTBI-induced AD-related pathogenesis, because rTBI induced AT8-positive puncta to a much lower extent in young (3 months) (Fig. 7I and fig. S18B) than in aged WT (8 months) mice (Fig. 6B and fig. S13A). This may reflect an age-dependent impairment in the cellular protein quality control system, as has been reported in the literature (44–47). That younger PS19 or WT mice that received exogenous tau seeds generally showed increases in tau pathology at earlier times after rTBI than did sham mice is consistent with the hypothesis that the younger mice have an ability to ultimately clear some misfolded tau species.

It is interesting that we consistently observed oligodendrocyte tau pathogenesis in our seeded rTBI model using the pathological tau seeds from four different AD cases, which all have glial-like tau pathology in white matter region (fig. S8). It has been recognized that changes in white matter are associated with AD onset and progression (48); however, the detailed associations and the underlying mechanisms need to be studied further. Whether the human white matter pathological tau is an unrecognized unique AD pathological tau strain that can induce glial tau pathogenesis, or whether it is a comorbid FTLD–like pathological tau strain that is capable of seeding oligodendrocyte tau pathology in WT mice (16, 49), is unknown and remains to be studied. It is notable that glial tau pathologies are very common in CTE brains (2), so the rTBI-induced oligodendrocyte tau pathology (Fig. 5, G to I, and figs. S12, A and E, and S18, C and G) might also result from unique tau species that are formed after rTBI and can seed oligodendrocyte tau pathology, or rTBI increased tau expression in oligodendrocytes so that they are more prone to tau pathology formation after seed uptake. We did not observe oligodendrocyte tau pathology in the optic tracts of WT mice that received rTBI without AD-tau injection, which may indicate that the observed oligodendrocyte tau pathology was seeded by the human brain–derived pathological tau preparation. In this study, we show that TBI can promote oligodendrocyte tau pathology, indicating an effect of TBI on tau pathologies in different cell types. This is consistent with a recent finding that transmission of oligodendrocyte tau pathology is not affected by neuronal tau ablation (49), suggesting that TBI-mediated tau pathology formation may occur independently in oligodendrocytes and neurons.

Distinct comorbid pathologies exist extensively in neurodegenerative diseases (34, 50–53). In our study, we observed the coexistence of tau and TDP43 pathologies in the optic tracts of rTBI-treated mice. The causal mechanism underlying TBI-induced cytoplasmic phosphorylated TDP43 accumulation is puzzling, because TDP43 is normally localized in the nucleus and is not known to bind microtubules. Previous reports have shown that stathmin-2, a microtubule regulator, connects TDP43 to axonal dysfunction (54, 55). However, whether microtubule disruption itself leads to TDP43 pathogenesis is unknown. We found that treatment with CNDR51657 could partially mitigate TBI-induced cytoplasmic TDP43 pathogenesis in the optic tracts. Because CNDR51657 treatment also lowered tau pathology, which preceded but often colocalized with TDP43 pathology, it is possible that the reduction of TBI-induced tau inclusions led to the decrease of TDP43 aggregates. Consistent with this speculation, other reports have suggested connections between TDP43 and tau protein, including the stress granule protein TIA-1 (56).

Prior studies on the effect of rTBI in WT or tau transgenic mice found relatively little tau pathology (25, 57–66), in contrast to the results obtained in our rTBI mouse models. Although we could not definitively rule out the possibility that some punctate staining might represent degenerating axons or neoantigens instead of tau, it is unlikely based on multiple pieces of evidence: (i) Immunostaining with different tau antibodies confirmed the nature of pathological tau forms (Fig. 6, A and G, and figs. S13B, S14A, and S16, B and C); (ii) sequential biochemical extraction of the optic nerve tissues from the mice with or without rTBI treatment showed that insoluble tau was enriched in the TBI-treated group (figs. S13C and S14B); (iii) the rTBI-mTauKO mice did not show AT8 puncta immunostaining as was observed in rTBI-WT mice (fig. S17J); and (iv) immunostaining with other antibodies, such as NFL, TA51 (Figs. 6D and 7D), pTDP43 (fig. S17D), and pSyn (fig. S17H), did not show the same pattern. It was very unlikely that rTBI-induced tau pathology in our study was confounded by effects of anesthesia or hypothermia (67, 68), because this was controlled by using the same surgical conditions for both sham and rTBI treatments. Similarly, we minimized other potential confounds by using the same genotype and age of mice with or without rTBI treatment. Thus, the more prominent tau pathology observed in our studies relative to prior reports likely relates to differences in mouse models and the implementation of different TBI paradigms. We found that the optic nerve and the connected optic tract are selectively vulnerable in both our seeded and nonseeded rTBI-WT mouse models, with the development of endogenous tau and TDP43 pathology and associated neurodegeneration that correlates with the post-rTBI period. The vulnerability of the optic tract to TBI damage has also been reported by others (32, 69, 70), and the underlying mechanisms require further study. The TBI paradigm might cause a coup-contrecoup injury so that certain regions distant from the site of impact, such as the optic tract, bear more of the shear force damage that is thought to play a key role in rTBI-related axonal pathogenesis (71) than do areas nearer the impact site, corresponding with a previous report (72). Glaucoma, which is caused by elevated eye pressure, shares some similar characteristics to our rTBI findings, including damage to the optic nerve (as well as retinal ganglia cells) and the deposition of tau (73, 74). In contrast to the optic tract, we did not detect AT8-positive tau pathology in the cortical regions and Cc of rTBI-WT mice, where axonal damage was not as obvious as in the optic tract.

Although our studies suggest that microtubule dysfunction is likely a key contributor to the accumulation and spread of pathologies in TBI/CTE, there are still many unknowns regarding the detailed mechanisms of how external brain forces lead to pathologic changes. In addition to microtubule disruption, rTBI-induced regional and cellular vulnerability may also account for the facilitated pathological tau transmission as shown in rTBI-PFF-PS19 (fig. S7) and rTBI-AD1-tau-WT mice (fig. S11). Moreover, injury-induced focal ischemia (75), hypoxia (76), calcium dysregulation (77–79), glial activation (80–82), and metabolic alternation (83–86) may also be involved in the connection between rTBI and protein pathogenesis.

Nonetheless, there are limitations to our study. For example, genetic drift in the PS19 mice since their first description has been noted (24), and there is sexual dimorphism in the PS19 model. Although the PS19 mice bred at our institution have developed delayed pathology onset over time, we continually examine the PS19 mice and find that, currently, males

predictably develop tau pathology starting at around 9 months of age. The differing tau pathology outcomes in rTBI-treated older male and female (7 months of age) PS19 mice (Fig. 3 and fig. S4A) likely reflect the greater tau expression observed in male than female PS19 mice. It is well known that tau protein expression influences tau pathogenesis in vivo (87–89) and that gender and age can influence the transgene expression in this model (fig. S4B and Fig. 3, E and F), as also reported by other groups who have used the PS19 line from the Jackson Laboratory (29–32). To address these known issues, we carefully controlled our experimental designs, including the use of the same generation of mice for all treatment groups within each study. The effects of rTBI were further validated in the AD-tau seeded WT mouse model (Fig. 5 and figs. S12 and S18, C to G), which represents the sporadic development of tau pathology independently of transgenes. In addition, the rTBI paradigm in this study could induce only punctate tau pathologies in nonseeded WT and APP-KI mice and not bona fide NFT pathology up to 9 m.p.t. This suggests that the rTBI protocol may be inadequate to induce enough endogenous pathological tau seeds to promote NFT formation, and we could overcome this limitation by preseeding WT mice with exogenous tau seeds before rTBI (Fig. 5). The absence of NFTs in rTBIWT mice may also reflect the limited number of impacts in our model or may require a longer observation post-injury interval to manifest. Moreover, it is likely that certain limitations of this model relate to the differences in size, architecture, and other risk factors between the mouse and human brain.

Meanwhile, we also acknowledge the potential side effects of preserving microtubules as a clinical intervention. It is reported that the doses of microtubule-stabilizing agents used for the treatment of cancer could elicit peripheral neuropathy and changes in blood cell division that manifest as neutropenia (90). These side effects would need to be monitored if drugs of this type were to be used in the treatment of neurodegenerative diseases, such as AD or CTE. However, prior studies from our laboratories (38, 91) and others (92) have revealed that the doses of microtubule-stabilizing compounds required to provide benefit in mouse tauopathy models are much lower than are needed for cancer treatment, and these low doses do not result in peripheral neuropathy or neutropenia. Thus, there is reason to believe that a therapeutic strategy of treating CTE or AD with microtubule-normalizing agents could be done safely.

In conclusion, in this study, we used multiple mouse models to explore the relationship between brain trauma and AD-related brain pathologies. These include both transgenic and WT mouse models with or without tau seeding, revealing that rTBI facilitates the development of protein pathogenesis, including tau and TDP43. Moreover, not only neuronal but also glial tau pathology is exacerbated by rTBI after intracerebral administration of exogenous tau seeds. Last, our data highlight the likely role of microtubule abnormalities in rTBI and the potential of microtubule-normalizing drugs as promising treatments for CTE and related neurodegenerative diseases.

MATERIALS AND METHODS

Study design

The overall objective of this study was to investigate the effects of rTBI on protein pathogenesis and neurodegeneration and to explore potential underlying mechanisms. To

this aim, different mouse models (including WT tau spreading models, PS19 tau transgenic mouse, and APP-KI mouse) were subjected to either rTBI or sham treatments, and tau pathogenesis, neurodegeneration, and associated protein pathologies were investigated. A brain-penetrant microtubule-stabilizing compound was used to preserve microtubule integrity. The rTBI experiments were conducted at the Interdisciplinary Research Center on Biology and Chemistry, Shanghai Institute of Organic Chemistry, Chinese Academy of Sciences, and the Center for Neurodegenerative Disease Research, University of Pennsylvania. Immunohistochemical staining was used to probe tau, TDP-43, α-Syn, and Aβ pathology in human and mouse brain tissue. The brain sections were imaged by a digital slide scanner, and the staining signals by different immunoreactive staining of tau or TDP-43 pathologies were quantified using software like HALO (Indica Labs) or QuPath software. Blind counts were made of the number of pathological cells, puncta, and microtubule density, and quantifications were systematically performed throughout the whole mouse brain. Semiquantitative analyses were conducted to create heatmaps representing the abundance and distributions of tau pathologies throughout the brain. The treatment of CNDR51657 was based on previous publications (38, 39). Open field, balance beam, and rotarod tests were used to measure the locomotor ability; light-dark box and elevated plus maze were used to measure the stress condition; and Y maze and Barnes maze were used to assess cognitive function of the rTBI-treated mice. Different treatments were blinded during the behavior tests, and the order of testing mice was randomized. The treatments were only revealed during the analysis of the data. The sample size was determined by power analysis based on previous studies (15, 16). All experiments were repeated with at least three biological replicates. No data points were excluded unless specified. Proper statistical analysis methods were performed to examine the differences between groups.

Supplementary Material

Refer to Web version on PubMed Central for supplementary material.

Acknowledgments:

We thank Y. Yao for PS19 mice characterization; J. Robinson, T. Schuck, and R. L. Changolkar from University of Pennsylvania for human brain tissue handling; and X. Wang from Center for Excellence in Brain Science and Intelligence Technology, Chinese Academy of Sciences for electron microscopy assistance. We thank P. Davies from Albert Einstein College of Medicine for contributing PHF-1 and MC1 antibodies. We also thank Y. Shen from University of Science and Technology of China, T. Wang from ShanghaiTech University, and K. He from Interdisciplinary Research Center on Biology and Chemistry, Shanghai Institute of Organic Chemistry, Chinese Academy of Sciences for providing help during the study, and E. Lee from University of Pennsylvania for helpful comments on the manuscript. We thank the staff members of the Animal Facility at the National Facility for Protein Science in Shanghai (NFPS), Shanghai Advanced Research Institute, Chinese Academy of Sciences, China for providing technical support and assistance in data collection and analysis.

Funding:

This work was supported by National Natural Science Foundation of China grant 82171413 (to Z.H.), Science and Technology Commission of Shanghai Municipality (STCSM) grants 21ZR1482900 (to Z.H.) and 2019SHZDZX02 (to Z.H.), and U.S. National Institutes of Health grants U19 AG062418 (to J.Q.T.), P01-AG17586 (to V.M.-Y.L.), and U01AG061173 (to K.R.B. and C.B.).

Data and materials availability:

All data associated with this study are present in the paper or the Supplementary Materials. CNDR51657 and tau PFFs can be respectively obtained from C.B. (University of California, San Diego) or Z.H. (Shanghai Institute of Organic Chemistry, Chinese Academy of Sciences) through a material transfer agreement.

REFERENCES AND NOTES

1. Lee VM, Goedert M, Trojanowski JQ, Neurodegenerative tauopathies. Annu. Rev. Neurosci. 24, 1121–1159 (2001). [PubMed: 11520930]
2. McKee AC, Cairns NJ, Dickson DW, Folkerth RD, Keene CD, Litvan I, Perl DP, Stein TD, Vonsattel JP, Stewart W, Tripodis Y, Crary JF, Bieniek KF, Dams-O'Connor K, Alvarez VE, Gordon WA, The first NINDS/NIBIB consensus meeting to define neuropathological criteria for the diagnosis of chronic traumatic encephalopathy. Acta Neuropathol. 131, 75–86 (2016). [PubMed: 26667418]
3. Avila J, Lucas JJ, Perez M, Hernandez F, Role of tau protein in both physiological and pathological conditions. Physiol. Rev. 84, 361–384 (2004). [PubMed: 15044677]
4. Goedert M, Eisenberg DS, Crowther RA, Propagation of tau aggregates and neurodegeneration. Annu. Rev. Neurosci. 40, 189–210 (2017). [PubMed: 28772101]
5. Shi Y, Zhang W, Yang Y, Murzin AG, Falcon B, Kotecha A, van Beers M, Tarutani A, Kametani F, Garringer HJ, Vidal R, Hallinan GI, Lashley T, Saito Y, Murayama S, Yoshida M, Tanaka H, Kakita A, Ikeuchi T, Robinson AC, Mann DMA, Kovacs GG, Revesz T, Ghetti B, Hasegawa M, Goedert M, Scheres SHW, Structure-based classification of tauopathies. Nature 598, 359–363 (2021). [PubMed: 34588692]
6. Braak H, Braak E, Neuropathological stageing of Alzheimer-related changes. Acta Neuropathol. 82, 239–259 (1991). [PubMed: 1759558]
7. Bennett DA, Schneider JA, Wilson RS, Bienias JL, Arnold SE, Neurofibrillary tangles mediate the association of amyloid load with clinical alzheimer disease and level of cognitive function. Arch. Neurol. 61, 378–384 (2004). [PubMed: 15023815]
8. McKhann GM, Albert MS, Grossman M, Miller B, Dickson D, Trojanowski JQ; Work Group on Frontotemporal Dementia and Pick's Disease, Clinical and pathological diagnosis of frontotemporal dementia: Report of the work group on frontotemporal dementia and Pick's disease. Arch. Neurol. 58, 1803–1809 (2001). [PubMed: 11708987]
9. Hoglinger GU, Respondek G, Stamelou M, Kurz C, Josephs KA, Lang AE, Mollenhauer B, Muller U, Nilsson C, Whitwell JL, Arzberger T, Englund E, Gelpi E, Giese A, Irwin DJ, Meissner WG, Pantelyat A, Rajput A, van Swieten JC, Troakes C, Antonini A, Bhatia KP, Bordelon Y, Compta Y, Corvol J-C, Colosimo C, Dickson DW, Dodel R, Ferguson L, Grossman M, Kassubek J, Krismer F, Levin J, Lorenzl S, Morris HR, Nestor P, Oertel WH, Poewe W, Rabinovici G, Rowe JB, Schellenberg GD, Seppi K, van Eimeren T, Wenning GK, Boxer AL, Golbe LI, Litvan I; Movement Disorder Society-endorsed PSP Study Group, Clinical diagnosis of progressive supranuclear palsy: The movement disorder society criteria. Mov. Disord. 32, 853–864 (2017). [PubMed: 28467028]
10. Mattay VS, Fera F, Tessitore A, Hariri AR, Das S, Callicott JH, Weinberger DR, Neurophysiological correlates of age-related changes in human motor function. Neurology 58, 630–635 (2002). [PubMed: 11865144]
11. Jucker M, Walker LC, Self-propagation of pathogenic protein aggregates in neurodegenerative diseases. Nature 501, 45–51 (2013). [PubMed: 24005412]
12. Iba M, Guo JL, McBride JD, Zhang B, Trojanowski JQ, Lee VM-Y, Synthetic tau fibrils mediate transmission of neurofibrillary tangles in a transgenic mouse model of Alzheimer's-like tauopathy. J. Neurosci. 33, 1024–1037 (2013). [PubMed: 23325240]
13. Guo JL, Narasimhan S, Changolkar L, He Z, Stieber A, Zhang B, Gathagan RJ, Iba M, McBride JD, Trojanowski JQ, Lee VMY, Unique pathological tau conformers from Alzheimer's brains transmit tau pathology in nontransgenic mice. J. Exp. Med. 213, 2635–2654 (2016). [PubMed: 27810929]
14. Narasimhan S, Guo JL, Changolkar L, Stieber A, McBride JD, Silva LV, He Z, Zhang B, Gathagan RJ, Trojanowski JQ, Lee VMY, Pathological tau strains from human brains recapitulate the

diversity of tauopathies in nontransgenic mouse brain. J. Neurosci. 37, 11406–11423 (2017). [PubMed: 29054878]

15. He Z, Guo JL, McBride JD, Narasimhan S, Kim H, Changolkar L, Zhang B, Gathagan RJ, Yue C, Dengler C, Stieber A, Nitla M, Coulter DA, Abel T, Brunden KR, Trojanowski JQ, Lee VM-Y, Amyloid-β plaques enhance Alzheimer's brain tau-seeded pathologies by facilitating neuritic plaque tau aggregation. Nat. Med. 24, 29–38 (2018). [PubMed: 29200205]
16. He Z, McBride JD, Xu H, Changolkar L, Kim S-J, Zhang B, Narasimhan S, Gibbons GS, Guo JL, Kozak M, Schellenberg GD, Trojanowski JQ, Lee VM-Y, Transmission of tauopathy strains is independent of their isoform composition. Nat. Commun. 11, 7 (2020). [PubMed: 31911587]
17. Xu D, Zhao H, Jin M, Zhu H, Shan B, Geng J, Dziedzic SA, Amin P, Mifflin L, Naito MG, Najafov A, Xing J, Yan L, Liu J, Qin Y, Hu X, Wang H, Zhang M, Manuel VJ, Tan L, He Z, Sun ZJ, Lee VMY, Wagner G, Yuan J, Modulating TRADD to restore cellular homeostasis and inhibit apoptosis. Nature 587, 133–138 (2020). [PubMed: 32968279]
18. Weitzman SA, Narasimhan S, He Z, Changolkar L, McBride JD, Zhang B, Schellenberg GD, Trojanowski JQ, Lee VMY, Insoluble tau from human FTDP-17 cases exhibit unique transmission properties in vivo. J. Neuropathol. Exp. Neurol. 79, 941–949 (2020). [PubMed: 32838419]
19. Darwich NF, Phan JM, Kim B, Suh E, Papatriantafyllou JD, Changolkar L, Nguyen AT, O'Rourke CM, He Z, Porta S, Gibbons GS, Luk KC, Papageorgiou SG, Grossman M, Massimo L, Irwin DJ, McMillan CT, Nasrallah IM, Toro C, Aguirre GK, Van Deerlin VM, Lee EB, Autosomal dominant VCP hypomorph mutation impairs disaggregation of PHF-tau. Science 370, eaay8826 (2020).
20. Gotz J, Halliday G, Nisbet RM, Molecular pathogenesis of the tauopathies. Annu. Rev. Pathol. 14, 239–261 (2019). [PubMed: 30355155]
21. Omalu BI, DeKosky ST, Minster RL, Kamboh MI, Hamilton RL, Wecht CH, Chronic traumatic encephalopathy in a National Football League player. Neurosurgery 57, 128–134 (2005).
22. McKee AC, Cantu RC, Nowinski CJ, Hedley-Whyte ET, Gavett BE, Budson AE, Santini VE, Lee HS, Kubilus CA, Stern RA, Chronic traumatic encephalopathy in athletes: Progressive tauopathy after repetitive head injury. J. Neuropathol. Exp. Neurol. 68, 709–735 (2009). [PubMed: 19535999]
23. Arena JD, Smith DH, Lee EB, Gibbons GS, Irwin DJ, Robinson JL, Lee VM-Y, Trojanowski JQ, Stewart W, Johnson VE, Tau immunophenotypes in chronic traumatic encephalopathy recapitulate those of ageing and Alzheimer's disease. Brain 143, 1572–1587 (2020). [PubMed: 32390044]
24. Yoshiyama Y, Higuchi M, Zhang B, Huang S-M, Iwata N, Saido TC, Maeda J, Suhara T, Trojanowski JQ, Lee VM-Y, Synapse loss and microglial activation precede tangles in a P301S tauopathy mouse model. Neuron 53, 337–351 (2007). [PubMed: 17270732]
25. Shitaka Y, Tran HT, Bennett RE, Sanchez L, Levy MA, Dikranian K, Brody DL, Repetitive closed-skull traumatic brain injury in mice causes persistent multifocal axonal injury and microglial reactivity. J. Neuropathol. Exp. Neurol. 70, 551–567 (2011). [PubMed: 21666502]
26. Huh JW, Widing AG, Raghupathi R, Midline brain injury in the immature rat induces sustained cognitive deficits, bihemispheric axonal injury and neurodegeneration. Exp. Neurol. 213, 84–92 (2008). [PubMed: 18599043]
27. Mouzon B, Chaytow H, Crynen G, Bachmeier C, Stewart J, Mullan M, Stewart W, Crawford F, Repetitive mild traumatic brain injury in a mouse model produces learning and memory deficits accompanied by histological changes. J. Neurotrauma 29, 2761–2773 (2012). [PubMed: 22900595]
28. Schmidt ML, Carden MJ, Lee VM, Trojanowski JQ, Phosphate dependent and independent neurofilament epitopes in the axonal swellings of patients with motor neuron disease and controls. Lab. Invest. 56, 282–294 (1987). [PubMed: 2434727]
29. Yanamandra K, Kfoury N, Jiang H, Mahan TE, Ma S, Maloney SE, Wozniak DF, Diamond MI, Holtzman DM, Anti-tau antibodies that block tau aggregate seeding in vitro markedly decrease pathology and improve cognition in vivo. Neuron 80, 402–414 (2013). [PubMed: 24075978]
30. Sun Y, Guo Y, Feng X, Jia M, Ai N, Dong Y, Zheng Y, Fu L, Yu B, Zhang H, Wu J, Yu X, Wu H, Kong W, The behavioural and neuropathologic sexual dimorphism and absence of MIP-3α in tau P301S mouse model of Alzheimer's disease. J. Neuroinflammation 17, 72 (2020). [PubMed: 32093751]

31. Ou W, Yang J, Simanauskaite J, Choi M, Castellanos DM, Chang R, Sun J, Jagadeesan N, Parfitt KD, Cribbs DH, Sumbria RK, Biologic TNF-α inhibitors reduce microgliosis, neuronal loss, and tau phosphorylation in a transgenic mouse model of tauopathy. J. Neuroinflammation 18, 312 (2021). [PubMed: 34972522]
32. Ramirez P, Zuniga G, Sun W, Beckmann A, Ochoa E, DeVos SL, Hyman B, Chiu G, Roy ER, Cao W, Orr M, Buggia-Prevot V, Ray WJ, Frost B, Pathogenic tau accelerates aging-associated activation of transposable elements in the mouse central nervous system. Prog. Neurobiol. 208, 102181 (2022).
33. Saito T, Matsuba Y, Mihira N, Takano J, Nilsson P, Itohara S, Iwata N, Saido TC, Single App knock-in mouse models of Alzheimer's disease. Nat. Neurosci. 17, 661–663 (2014). [PubMed: 24728269]
34. Josephs KA, Whitwell JL, Weigand SD, Murray ME, Tosakulwong N, Liesinger AM, Petrucelli L, Senjem ML, Knopman DS, Boeve BF, Ivnik RJ, Smith GE, Jack CR Jr., Parisi JE, Petersen RC, Dickson DW, TDP-43 is a key player in the clinical features associated with Alzheimer's disease. Acta Neuropathol. 127, 811–824 (2014). [PubMed: 24659241]
35. Dawson HN, Cantillana V, Jansen M, Wang H, Vitek MP, Wilcock DM, Lynch JR, Laskowitz DT, Loss of tau elicits axonal degeneration in a mouse model of Alzheimer's disease. Neuroscience 169, 516–531 (2010). [PubMed: 20434528]
36. Dawson HN, Ferreira A, Eyster MV, Ghoshal N, Binder LI, Vitek MP, Inhibition of neuronal maturation in primary hippocampal neurons from tau deficient mice. J. Cell Sci. 114, 1179–1187 (2001). [PubMed: 11228161]
37. Kovalevich J, Cornec A-S, Yao Y, James M, Crowe A, Lee VM-Y, Trojanowski JQ, Smith AB III, Ballatore C, Brunden KR, Characterization of brain-penetrant pyrimidine-containing molecules with differential microtubule-stabilizing activities developed as potential therapeutic agents for Alzheimer's disease and related tauopathies. J. Pharmacol. Exp. Ther. 357, 432–450 (2016). [PubMed: 26980057]
38. Zhang B, Yao Y, Cornec A-S, Oukoloff K, James MJ, Koivula P, Trojanowski JQ, Smith AB III, Lee VM-Y, Ballatore C, Brunden KR, A brain-penetrant triazolopyrimidine enhances microtubule-stability, reduces axonal dysfunction and decreases tau pathology in a mouse tauopathy model. Mol. Neurodegener. 13, 59 (2018). [PubMed: 30404654]
39. Yao Y, Nzou G, Alle T, Tsering W, Maimaiti S, Trojanowski JQ, Lee VM-Y, Ballatore C, Brunden KR, Correction of microtubule defects within Aβ plaque-associated dystrophic axons results in lowered Aβ release and plaque deposition. Alzheimers Dement. 16, 1345–1357 (2020). [PubMed: 32918367]
40. Seabrook TA, Burbridge TJ, Crair MC, Huberman AD, Architecture, function, and assembly of the mouse visual system. Annu. Rev. Neurosci. 40, 499–538 (2017). [PubMed: 28772103]
41. Zanier ER, Bertani I, Sammali E, Pischiutta F, Chiaravalloti MA, Vegliante G, Masone A, Corbelli A, Smith DH, Menon DK, Stocchetti N, Fiordaliso F, De Simoni MG, Stewart W,Chiesa R, Induction of a transmissible tau pathology by traumatic brain injury. Brain 141, 2685–2699 (2018). [PubMed: 30084913]
42. Kochl R, Hu XW, Chan EYW, Tooze SA, Microtubules facilitate autophagosome formation and fusion of autophagosomes with endosomes. Traffic 7, 129–145 (2006). [PubMed: 16420522]
43. Falzone TL, Gunawardena S, McCleary D, Reis GF, Goldstein LSB, Kinesin-1 transport reductions enhance human tau hyperphosphorylation, aggregation and neurodegeneration in animal models of tauopathies. Hum. Mol. Genet. 19, 4399–4408 (2010). [PubMed: 20817925]
44. Balch WE, Morimoto RI, Dillin A, Kelly JW, Adapting proteostasis for disease intervention. Science 319, 916–919 (2008). [PubMed: 18276881]
45. Douglas PM, Dillin A, Protein homeostasis and aging in neurodegeneration. J. Cell Biol. 190, 719–729 (2010). [PubMed: 20819932]
46. Taylor RC, Dillin A, Aging as an event of proteostasis collapse. Cold Spring Harb. Perspect. Biol. 3, a004440 (2011).
47. Santra M, Dill KA, de Graff AMR, Proteostasis collapse is a driver of cell aging and death. Proc. Natl. Acad. Sci. U.S.A. 116, 22173–22178 (2019). [PubMed: 31619571]

48. Xu MY, Xu ZQ, Wang YJ, White matter “matters” in Alzheimer’s disease. Neurosci. Bull. 38, 323–326 (2022). [PubMed: 34854054]
49. Narasimhan S, Changolkar L, Riddle DM, Kats A, Stieber A, Weitzman SA, Zhang B, Li Z, Roberson ED, Trojanowski JQ, Lee VMY, Human tau pathology transmits glial tau aggregates in the absence of neuronal tau. J. Exp. Med. 217, e20190783 (2020).
50. Lippa CF, Fujiwara H, Mann DM, Giasson B, Baba M, Schmidt ML, Nee LE, O’Connell B, Pollen DA, St George-Hyslop P, Ghetti B, Nochlin D, Bird TD, Cairns NJ, Lee VM, Iwatsubo T, Trojanowski JQ, Lewy bodies contain altered alpha-synuclein in brains of many familial Alzheimer’s disease patients with mutations in presenilin and amyloid precursor protein genes. Am. J. Pathol. 153, 1365–1370 (1998). [PubMed: 9811326]
51. Hamilton RL, Lewy bodies in Alzheimer’s disease: A neuropathological review of 145 cases using alpha-synuclein immunohistochemistry. Brain Pathol. 10, 378–384 (2000). [PubMed: 10885656]
52. Arai Y, Yamazaki M, Mori O, Muramatsu H, Asano G, Katayama Y, Alpha-synuclein-positive structures in cases with sporadic Alzheimer’s disease: Morphology and its relationship to tau aggregation. Brain Res. 888, 287–296 (2001). [PubMed: 11150486]
53. Robinson JL, Lee EB, Xie SX, Rennert L, Suh E, Bredenberg C, Caswell C, Van Deerlin VM, Yan N, Yousef A, Hurtig HI, Siderowf A, Grossman M, McMillan CT, Miller B, Duda JE, Irwin DJ, Wolk D, Elman L, McCluskey L, Chen-Plotkin A, Weintraub D, Arnold SE, Brettschneider J, Lee VM, Trojanowski JQ, Neurodegenerative disease concomitant proteinopathies are prevalent, age-related and APOE4-associated. Brain 141, 2181–2193 (2018). [PubMed: 29878075]
54. Klim JR, Williams LA, Limone F, Juan IGS, Davis-Dusenbery BN, Mordes DA, Burberry A, Steinbaugh MJ, Gamage KK, Kirchner R, Moccia R, Cassel SH, Chen K, Wainger BJ, Woolf CJ, Eggan K, ALS-implicated protein TDP-43 sustains levels of STMN2, a mediator of motor neuron growth and repair. Nat. Neurosci. 22, 167–179 (2019). [PubMed: 30643292]
55. Melamed Z, Lopez-Erauskin J, Baughn MW, Zhang O, Drenner K, Sun Y, Freyermuth F, McMahon MA, Beccari MS, Artates JW, Ohkubo T, Rodriguez M, Lin N, Wu D, Bennett CF, Rigo F, Da Cruz S, Ravits J, Lagier-Tourenne C, Cleveland DW, Premature polyadenylation-mediated loss of stathmin-2 is a hallmark of TDP-43-dependent neurodegeneration. Nat. Neurosci. 22, 180–190 (2019). [PubMed: 30643298]
56. McDonald KK, Aulas A, Destroismaisons L, Pickles S, Beleac E, Camu W, Rouleau GA, Vande Velde C, TAR DNA-binding protein 43 (TDP-43) regulates stress granule dynamics via differential regulation of G3BP and TIA-1. Hum. Mol. Genet. 20, 1400–1410 (2011). [PubMed: 21257637]
57. Kanayama G, Takeda M, Niigawa H, Ikura Y, Tamii H, Taniguchi N, Kudo T, Miyamae Y, Morihara T, Nishimura T, The effects of repetitive mild brain injury on cytoskeletal protein and behavior. Methods Find. Exp. Clin. Pharmacol. 18, 105–115 (1996). [PubMed: 8740242]
58. Laurer HL, Bareyre FM, Lee VM, Trojanowski JQ, Longhi L, Hoover R, Saatman KE, Raghupathi R, Hoshino S, Grady MS, McIntosh TK, Mild head injury increasing the brain’s vulnerability to a second concussive impact. J. Neurosurg. 95, 859–870 (2001). [PubMed: 11702878]
59. DeFord SM, Wilson MS, Rice AC, Clausen T, Rice LK, Barabnova A, Bullock R, Hamm RJ, Repeated mild brain injuries result in cognitive impairment in B6C3F1 mice. J. Neurotrauma 19, 427–438 (2002). [PubMed: 11990349]
60. Creeley CE, Wozniak DF, Bayly PV, Olney JW, Lewis LM, Multiple episodes of mild traumatic brain injury result in impaired cognitive performance in mice. Acad. Emerg. Med. 11, 809–819 (2004). [PubMed: 15289185]
61. Longhi L, Saatman KE, Fujimoto S, Raghupathi R, Meaney DF, Davis J, McMillan B A. Conte S,V, Laurer HL, Stein S, Stocchetti N, McIntosh TK, Temporal window of vulnerability to repetitive experimental concussive brain injury. Neurosurgery 56, 364–374 (2005). [PubMed: 15670384]
62. Friess SH, Ichord RN, Ralston J, Ryall K, Helfaer MA, Smith C, Margulies SS, Repeated traumatic brain injury affects composite cognitive function in piglets. J. Neurotrauma 26, 1111–1121 (2009). [PubMed: 19275468]
63. Meehan III WP, Zhang J, Mannix R, Whalen MJ, Increasing recovery time between injuries improves cognitive outcome after repetitive mild concussive brain injuries in mice. Neurosurgery 71, 885–891 (2012). [PubMed: 22743360]

64. Mouzon BC, Bachmeier C, Ferro A, Ojo JO, Crynen G, Acker CM, Davies P, Mullan M, Stewart W, Crawford F, Chronic neuropathological and neurobehavioral changes in a repetitive mild traumatic brain injury model. Ann. Neurol. 75, 241–254 (2014). [PubMed: 24243523]

65. Petraglia AL, Plog BA, Dayawansa S, Chen M, Dashnaw ML, Czerniecka K, Walker CT, Viterise T, Hyrien O, Iliff JJ, Deane R, Nedergaard M, Huang JH, The spectrum of neurobehavioral sequelae after repetitive mild traumatic brain injury: A novel mouse model of chronic traumatic encephalopathy. J. Neurotrauma 31, 1211–1224 (2014). [PubMed: 24766454]

66. Brody DL, Benetatos J, Bennett RE, Klemenhagen KC, Mac Donald CL, The pathophysiology of repetitive concussive traumatic brain injury in experimental models; new developments and open questions. Mol. Cell. Neurosci. 66, 91–98 (2015). [PubMed: 25684677]

67. Planel E, Richter KEG, Nolan CE, Finley JE, Liu L, Wen Y, Krishnamurthy P, Herman M, Wang L, Schachter JB, Nelson RB, Lau L-F, Duff KE, Anesthesia leads to tau hyperphosphorylation through inhibition of phosphatase activity by hypothermia. J. Neurosci. 27, 3090–3097 (2007). [PubMed: 17376970]

68. El Khoury NB, Gratuze M, Petry F, Papon MA, Julien C, Marcouiller F, Morin F, Nicholls SB, Calon F, Hebert SS, Marette A, Planel E, Hypothermia mediates age-dependent increase of tau phosphorylation in db/db mice. Neurobiol. Dis. 88, 55–65 (2016). [PubMed: 26777665]

69. Tzekov R, Quezada A, Gautier M, Biggins D, Frances C, Mouzon B, Jamison J, Mullan M, Crawford F, Repetitive mild traumatic brain injury causes optic nerve and retinal damage in a mouse model. J. Neuropathol. Exp. Neurol. 73, 345–361 (2014). [PubMed: 24607965]

70. Evanson NK, Guilhaume-Correa F, Herman JP, Goodman MD, Optic tract injury after closed head traumatic brain injury in mice: A model of indirect traumatic optic neuropathy. PLOS ONE 13, e0197346 (2018).

71. Smith DH, Meaney DF, Axonal damage in traumatic brain injury. Neuroscientist 6, 483–495 (2000).

72. Tagge CA, Fisher AM, Minaeva OV, Gaudreau-Balderrama A, Moncaster JA, Zhang XL, Wojnarowicz MW, Casey N, Lu H, Kokiko-Cochran ON, Saman S, Ericsson M, Onos KD, Veksler R, Senatorov VV Jr., Kondo A, Zhou XZ, Miry O, Vose LR, Gopaul KR, Upreti C, Nowinski CJ, Cantu RC, Alvarez VE, Hildebrandt AM, Franz ES, Konrad J, Hamilton JA, Hua N, Tripodis Y, Anderson AT, Howell GR, Kaufer D, Hall GF, Lu KP, Ransohoff RM, Cleveland RO, Kowall NW, Stein TD, Lamb BT, Huber BR, Moss WC, Friedman A, Stanton PK, McKee AC, Goldstein LE, Concussion, microvascular injury, and early tauopathy in young athletes after impact head injury and an impact concussion mouse model. Brain 141, 422–458 (2018). [PubMed: 29360998]

73. Chiasseu M, Cueva Vargas JL, Destroismaisons L, Vande Velde C, Leclerc N, Di Polo A, Tau accumulation, altered phosphorylation, and missorting promote deurodegeneration in glaucoma. Neuroscience 36, 5785–5798 (2016). [PubMed: 27225768]

74. Sen S, Saxena R, Tripathi M, Vibha D, Dhiman R, Neurodegeneration in Alzheimer's disease and glaucoma: Overlaps and missing links. Eye (Lond.) 34, 1546–1553 (2020). [PubMed: 32152519]

75. Chang JJJ, Youn TS, Benson D, Mattick H, Andrade N, Harper CR, Moore CB, Madden CJ, Diaz-Arrastia RR, Physiologic and functional outcome correlates of brain tissue hypoxia in traumatic brain injury. Crit. Care Med. 37, 283–290 (2009). [PubMed: 19050612]

76. Wouters BG, Koritzinsky M, Hypoxia signalling through mTOR and the unfolded protein response in cancer. Nat. Rev. Cancer 8, 851–864 (2008). [PubMed: 18846101]

77. Saito K, Elce JS, Hamos JE, Nixon RA, Widespread activation of calcium-activated neutral proteinase (calpain) in the brain in Alzheimer disease: A potential molecular basis for neuronal degeneration. Proc. Natl. Acad. Sci. U.S.A. 90, 2628–2632 (1993). [PubMed: 8464868]

78. Kurbatskaya K, Phillips EC, Croft CL, Dentoni G, Hughes MM, Wade MA, Al-Sarraj S, Troakes C, O'Neill MJ, Perez-Nievas BG, Hanger DP, Noble W, Upregulation of calpain activity precedes tau phosphorylation and loss of synaptic proteins in Alzheimer's disease brain. Acta Neuropathol. Commun. 4, 34 (2016). [PubMed: 27036949]

79. Wang Y, Liu Y, Nham A, Sherbaf A, Quach D, Yahya E, Ranburger D, Bi X, Baudry M, Calpain-2 as a therapeutic target in repeated concussion-induced neuropathy and behavioral impairment. Sci. Adv. 6, eaba5547 (2020).

80. Simon DW, McGeachy MJ, Bayir H, Clark RSB, Loane DJ, Kochanek PM, The far-reaching scope of neuroinflammation after traumatic brain injury. Nat. Rev. Neurol. 13, 572 (2017). [PubMed: 28776601]
81. Kinney JW, Bemiller SM, Murtishaw AS, Leisgang AM, Salazar AM, Lamb BT, Inflammation as a central mechanism in Alzheimer's disease. Alzheimers Dement. (N Y) 4, 575–590 (2018). [PubMed: 30406177]
82. Laurent C, Buee L, Blum D, Tau and neuroinflammation: What impact for Alzheimer's disease and tauopathies? Biomed. J. 41, 21–33 (2018). [PubMed: 29673549]
83. Adibhatla RM, Hatcher JF, Altered lipid metabolism in brain injury and disorders. Subcell. Biochem. 49, 241–268 (2008). [PubMed: 18751914]
84. Prins ML, Cerebral metabolic adaptation and ketone metabolism after brain injury. J. Cereb. Blood Flow Metab. 28, 1–16 (2008). [PubMed: 17684514]
85. Liu F, Shi J, Tanimukai H, Gu J, Gu J, Grundke-Iqbal I, Iqbal K, Gong CX, Reduced O-GlcNAcylation links lower brain glucose metabolism and tau pathology in Alzheimer's disease. Brain 132, 1820–1832 (2009). [PubMed: 19451179]
86. Xu XJ, Yang MS, Zhang B, Niu F, Dong JQ, Liu BY, Glucose metabolism: A link between traumatic brain injury and Alzheimer's disease. Chin. J. Traumatol. 24, 5–10 (2021). [PubMed: 33358332]
87. Santacruz K, Lewis J, Spires T, Paulson J, Kotilinek L, Ingelsson M, Guimaraes A, DeTure M, Ramsden M, McGowan E, Forster C, Yue M, Orne J, Janus C, Mariash A, Kuskowski M, Hyman B, Hutton M, Ashe KH, Tau suppression in a neurodegenerative mouse model improves memory function. Science 309, 476–481 (2005). [PubMed: 16020737]
88. Adams SJ, Crook RJP, DeTure M, Randle SJ, Innes AE, Yu XZ, Lin W-L, Dugger BN, McBride M, Hutton M, Dickson DW, McGowan E, Overexpression of wild-type murine tau results in progressive tauopathy and neurodegeneration. Am. J. Pathol. 175, 1598–1609 (2009). [PubMed: 19717642]
89. DeVos SL, Miller RL, Schoch KM, Holmes BB, Kebodeaux CS, Wegener AJ, Chen G, Shen T, Tran H, Nichols B, Zanardi TA, Kordasiewicz HB, Swayze EE, Bennett CF, Diamond MI, Miller TM, Tau reduction prevents neuronal loss and reverses pathological tau deposition and seeding in mice with tauopathy. Sci. Transl. Med. 9, eaag0481 (2017).
90. Mukhtar E, Adhami VM, Mukhtar H, Targeting microtubules by natural agents for cancer therapy. Mol. Cancer Ther. 13, 275–284 (2014). [PubMed: 24435445]
91. Zhang B, Carroll J, Trojanowski JQ, Yao Y, Iba M, Potuzak JS, Hogan A-ML, Xie SX, Ballatore C, Smith AB III, Lee VM-Y, Brunden KR, The microtubule-stabilizing agent, epothilone D, reduces axonal dysfunction, neurotoxicity, cognitive deficits, and Alzheimer-like pathology in an interventional study with aged tau transgenic mice. J. Neurosci. 32, 3601–3611 (2012). [PubMed: 22423084]
92. Barten DM, Fanara P, Andorfer C, Hoque N, Wong PY, Husted KH, Cadelina GW, Decarr LB, Yang L, Liu V, Fessler C, Protassio J, Riff T, Turner H, Janus CG, Sankaranarayanan S, Polson C, Meredith JE, Gray G, Hanna A, Olson RE, Kim S-H, Vite GD, Lee FY, Albright CF, Hyperdynamic microtubules, cognitive deficits, and pathology are improved in tau transgenic mice with low doses of the microtubule-stabilizing agent BMS-241027. J. Neurosci. 32, 7137–7145 (2012). [PubMed: 22623658]
93. Bugiani O, Murrell JR, Giaccone G, Hasegawa M, Ghigo G, Tabaton M, Morbin M, Primavera A, Carella F, Solaro C, Grisoli M, Savoiardo M, Spillantini MG, Tagliavini F, Goedert M, Ghetti B, Frontotemporal dementia and corticobasal degeneration in a family with a P301S mutation in tau. J. Neuropathol. Exp. Neurol. 58, 667–677 (1999). [PubMed: 10374757]
94. Guo JL, Lee VM-Y, Seeding of normal tau by pathological tau conformers drives pathogenesis of Alzheimer-like tangles. J. Biol. Chem. 286, 15317–15331 (2011). [PubMed: 21372138]
95. Kirkpatrick LL, Witt AS, Payne HR, Shine HD, Brady ST, Changes in microtubule stability and density in myelin-deficient shiverer mouse CNS axons. J. Neurosci. 21, 2288–2297 (2001). [PubMed: 11264304]
96. Yamada Y, Hada Y, Imamura K, Mataga N, Watanabe Y, Yamamoto M, Differential expression of immediate-early genes, c-fos and zif268, in the visual cortex of young rats: Effects of

a noradrenergic neurotoxin on their expression. Neuroscience 92, 473–484 (1999). [PubMed: 10408598]

97. Liu D, Deng J, Zhang Z, Zhang ZY, Sun YG, Yang T, Yao H, Orbitofrontal control of visual cortex gain promotes visual associative learning. Nat. Commun. 11, 2784 (2020). [PubMed: 32493971]
98. de Jong JW, Afjei SA, Pollak Dorocic I, Peck JR, Liu C, Kim CK, Tian L, Deisseroth K, Lammel S, A neural circuit mechanism for encoding aversive stimuli in the mesolimbic dopamine system. Neuron 101, 133–151.e7 (2019). [PubMed: 30503173]
99. Kovacs GG, Ferrer I, Grinberg LT, Alafuzoff I, Attems J, Budka H, Cairns NJ, Crary JF, Duyckaerts C, Ghetti B, Halliday GM, Ironside JW, Love S, Mackenzie IR, Munoz DG, Murray ME, Nelson PT, Takahashi H, Trojanowski JQ, Ansorge O, Arzberger T, Baborie A, Beach TG, Bieniek KF, Bigio EH, Bodi I, Dugger BN, Feany M, Gelpi E, Gentleman SM, Giaccone G, Hatanpaa KJ, Heale R, Hof PR, Hofer M, Hortobagyi T, Jellinger K, Jicha GA, Ince P, Kofler J, Kovari E, Kril JJ, Mann DM, Matej R, McKee AC, McLean C, Milenkovic I, Montine TJ, Murayama S, Lee EB, Rahimi J, Rodriguez RD, Rozemuller A, Schneider JA, Schultz C, Seeley W, Seilhean D, Smith C, Tagliavini F, Takao M, Thal DR, Toledo JB, Tolnay M, Troncoso JC, Vinters HV, Weis S, Wharton SB, White III CL, Wisniewski T, Woulfe JM, Yamada M, Dickson DW, Aging-related tau astrogliopathy (ARTAG): Harmonized evaluation strategy. Acta Neuropathol. 131, 87–102 (2016). [PubMed: 26659578]

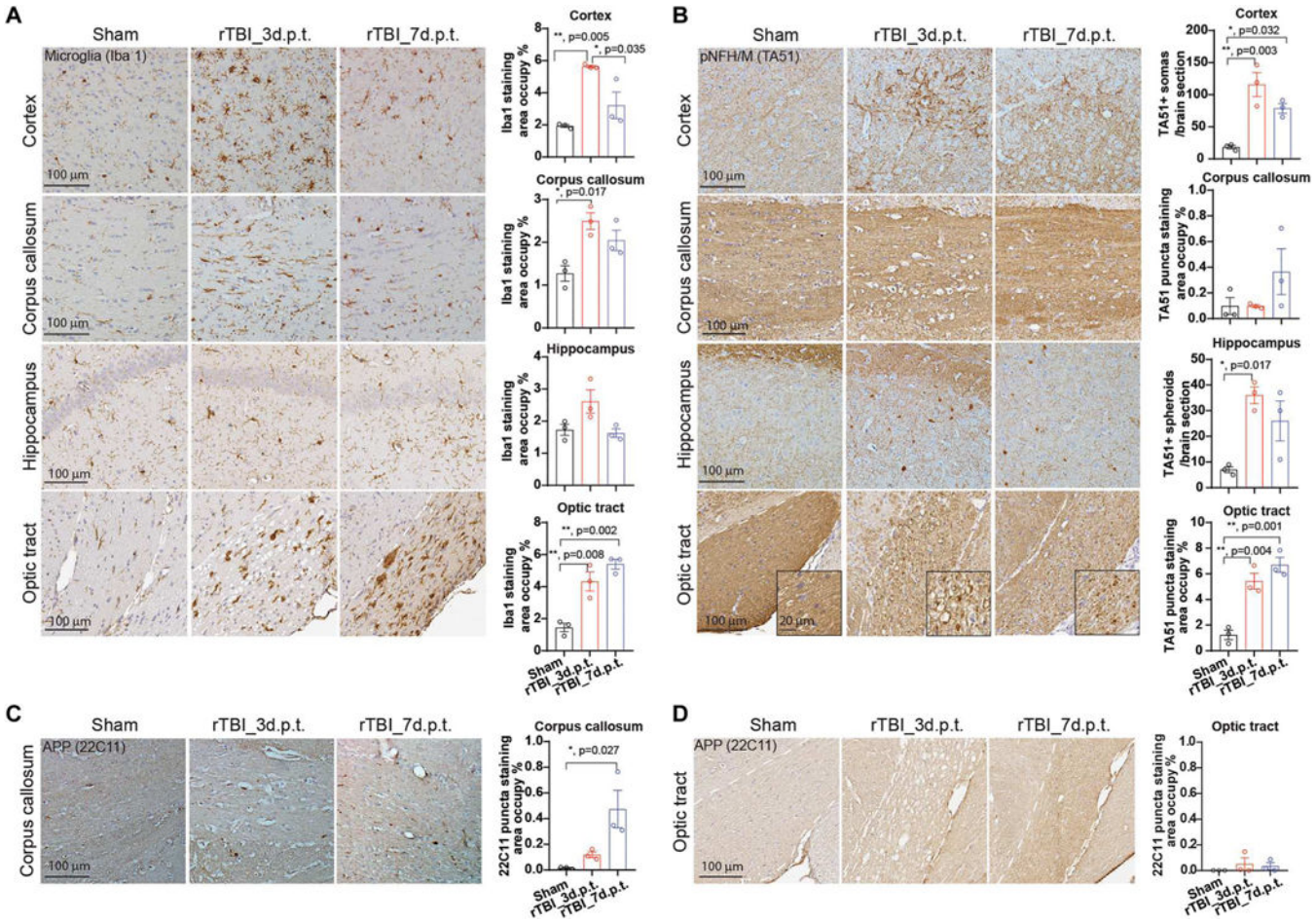

Fig. 1. The short-term effect of rTBI in old PS19 mice.

(**A**) (Left) Tissue sections were stained by immunohistochemistry using an antibody to Iba-1. Representative images of the cortex, Cc, hippocampus, and optic tract in sham- or rTBI-treated 7-month-old PS19 mice are shown. (Right) Bar graph summarizing the corresponding Iba-1 immunostaining from left and right hemispheres in sham- and rTBI-treated mice 3 and 7 d.p.t. (**B**) (Left) Representative images of immunohistochemistry staining using the TA51 antibody to label phospho-neurofilaments for the same brain areas as in (A). Insets are higher-magnified images of optic tracts. (Right) Bar graph summarizing the corresponding TA51 immunostaining in sham mice and rTBI mice 3 and 7 d.p.t. (**C**) (Left) Representative images of immunostaining with the anti-APP antibody 22C11 in the Cc. (Right) Bar graph summarizing the corresponding 22C11 immunostaining in sham mice and rTBI mice 3 and 7 d.p.t. (**D**) (Left) Representative images of immunostaining with the anti-APP antibody 22C11 in the optic tract. White dashed lines indicate the boundary of optic tracts. (Right) Bar graph summarizing the corresponding 22C11 immunostaining in sham mice and rTBI mice 3 and 7 d.p.t. $n = 3$ mice per group. Scale bars are indicated in the images. One-way analysis of variance (ANOVA) followed by Šidák's multiple comparisons was conducted for the statistical analysis. Data are presented as means ± SEM, with each symbol representing a mouse.

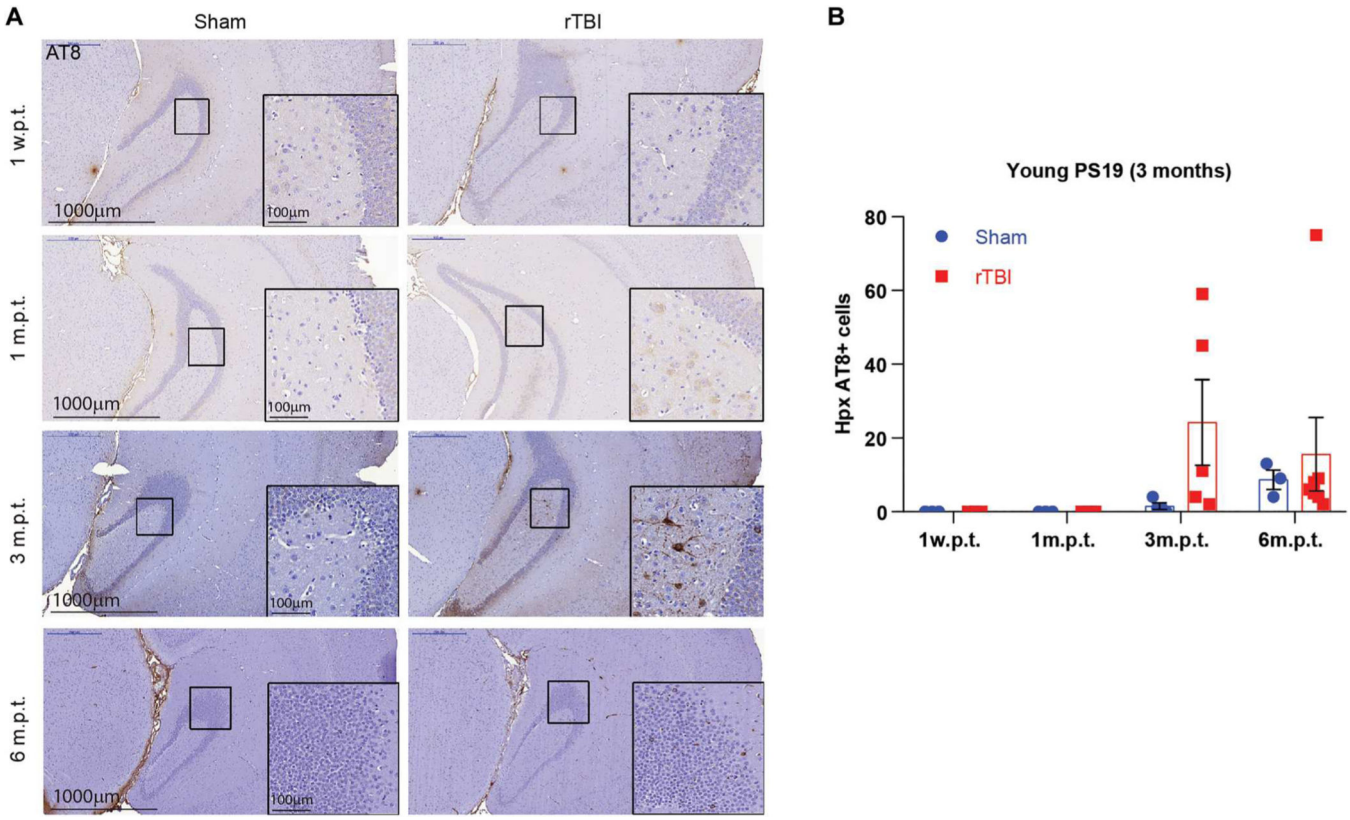

Fig. 2. The long-term effect of rTBI on tau pathogenesis in young male PS19 mice.

(**A**) Brain sections were stained by immunohistochemistry using the AT8 antibody to phosphorylated tau. Representative images of caudal hippocampal regions (Hpx) of the young 3-month-old sham-treated (left) and rTBI-treated (right) PS19 mice at different time points after treatment are shown. Insets are magnifications of indicated black squares; scale bars are indicated in the images. (**B**) Quantification of AT8-positive cells in (A). $n = 3$ to 7 mice per group. Two-way ANOVA was used to evaluate the rTBI effects. Data are presented as means ± SEM, with each symbol representing a mouse.

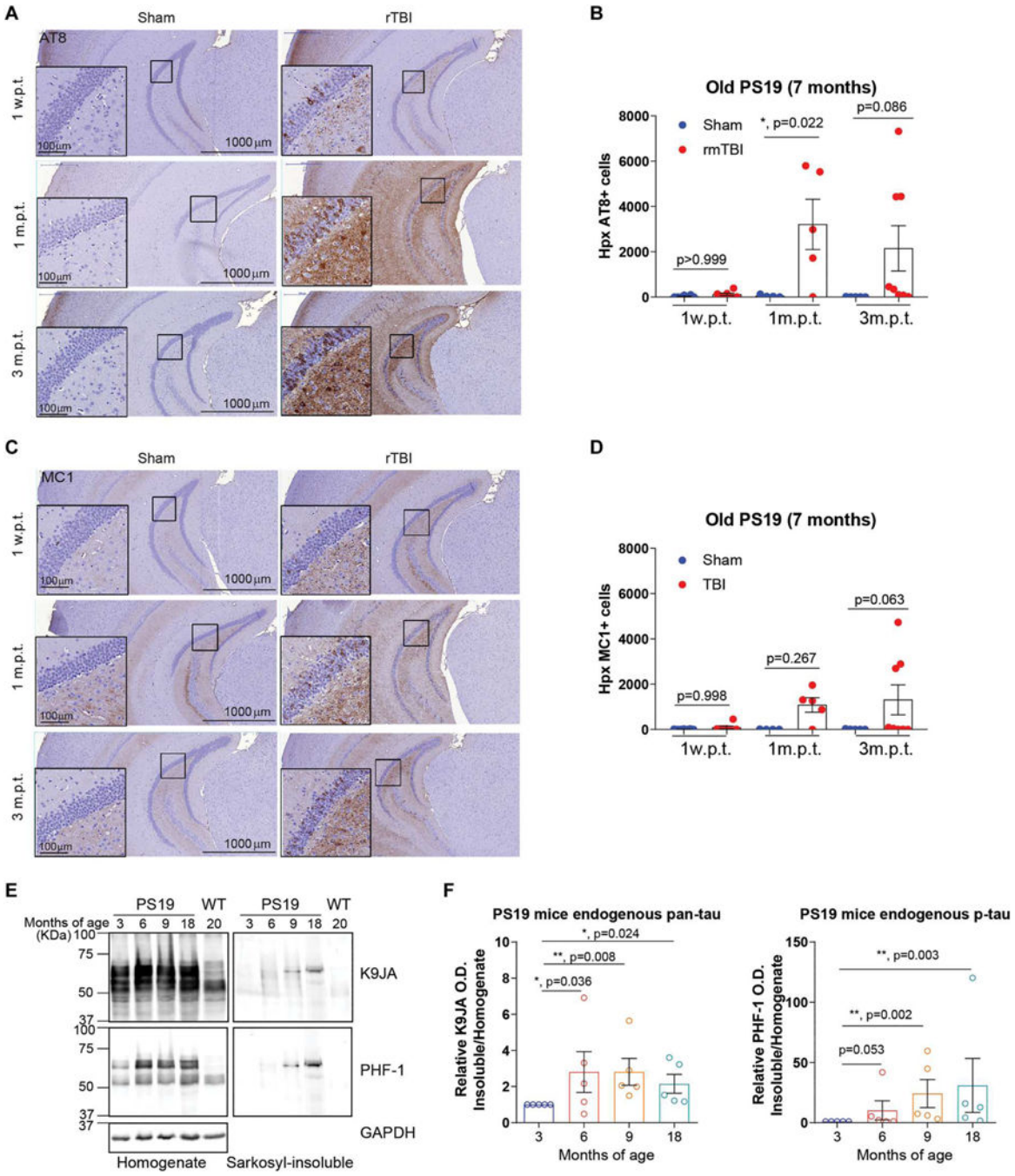

Fig. 3. The long-term effect of rTBI on tau pathogenesis in older male PS19 mice.

(**A**) Brain sections were stained by immunohistochemistry using the AT8 antibody to phosphorylated tau. Representative images of caudal hippocampal regions of 7-month-old sham (left) and rTBI (right) PS19 mice at different time points after treatment are shown. (**B**) Number of AT8-labeled cells in the hippocampus (Hpx). (**C**) Brain sections were stained by immunohistochemistry using the MC1 antibody to misfolded tau. Representative images of caudal hippocampal regions of 7-month-old sham-treated (left) and rTBI-treated (right) PS19 mice at different time points after treatment are shown. Insets are magnifications of

indicated black squares; scale bars are indicated in the images. (**D**) Number of MC1-labeled cells in the hippocampus. (**E**) Representative immunoblots of the sequential extraction from brain tissues at different ages of male PS19 mice. K9JA is a pan-tau antibody, and PHF-1 is an anti-phosphorylated tau antibody (pSer^{396}/Ser^{404}). Glyceraldehyde-3-phosphate dehydrogenase (GAPDH) was used as the loading control. Equal proportions of homogenate were analyzed for each sample, with a 25-fold greater amount of the corresponding sarkosyl-insoluble fraction loaded relative to the soluble fraction. (**F**) Quantification of relative insoluble total tau (left) and insoluble phosphorylated tau (right). n = 4 to 8 mice per group. Data are presented as means ± SEM, with each symbol representing a mouse. Two-way ANOVA followed by Šidák's multiple comparison tests was used to evaluate the rTBI effects within each time point in (B) and (D). One-way ANOVA (Kruskal-Wallis test) followed by Dunn's tests was used in (F).

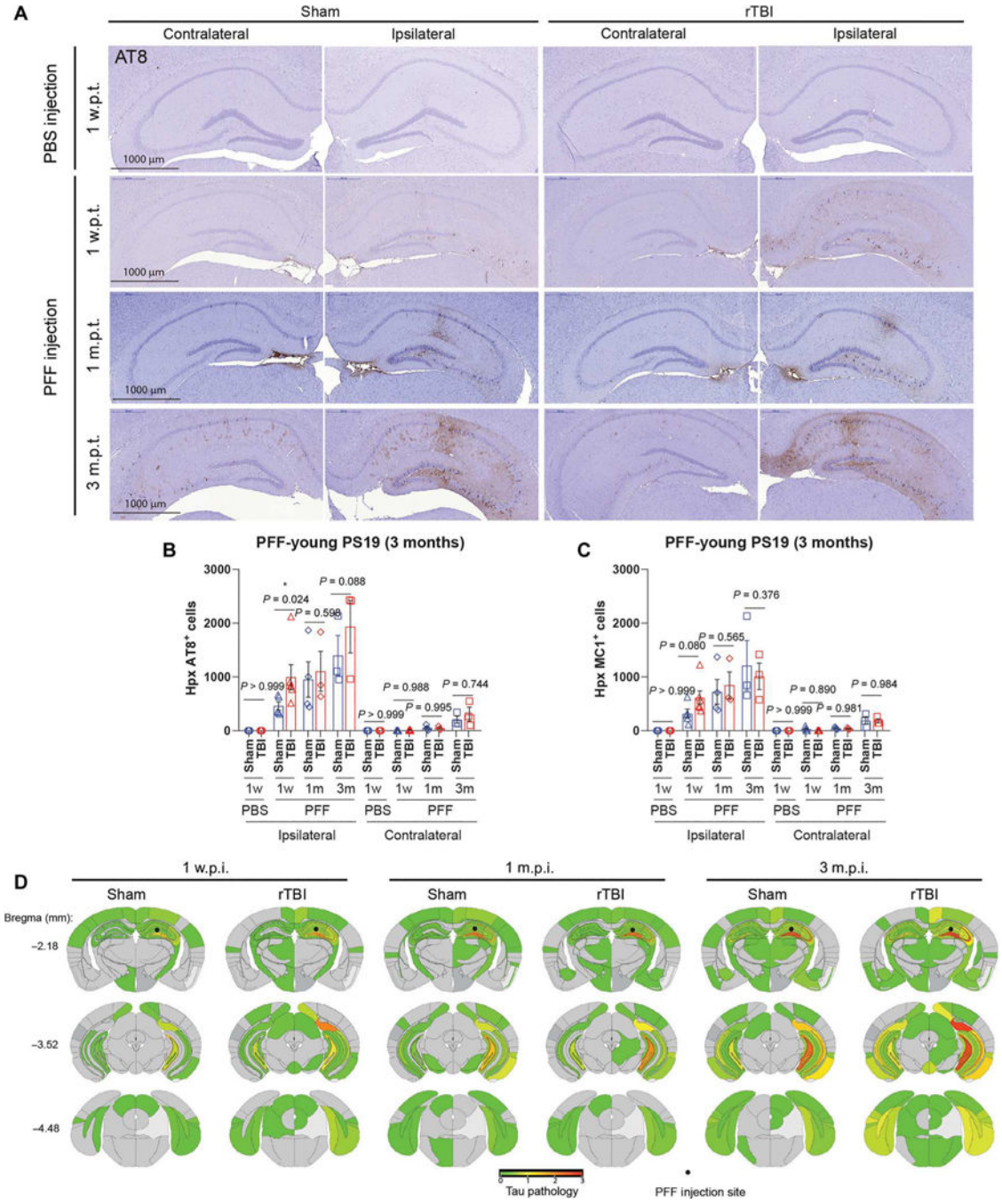

Fig. 4. rTBI accelerated tau pathogenesis in young PS19 mice preinoculated with synthetic tau PFFs.

(**A**) Brain sections were stained by immunohistochemistry using the AT8 antibody to phosphorylated tau. Representative images of dorsal hippocampal regions of 3-month-old sham-treated (left) or rTBI-treated (right) PS19 mice unilaterally preinoculated with PBS or synthetic tau PFFs at different time points after treatment are shown. Scale bars are indicated in the images. (**B**) Quantification of AT8-positive cells in the ipsilateral and contralateral hippocampal regions (Hpx) of each mouse as shown in (A). (**C**) Quantification of MC1-

positive cells in the ipsilateral and contralateral hippocampal regions of each sham or rTBI mouse preinoculated with PBS or tau PFFs at different time points after treatment. Data are presented as means ± SEM, and scatter plots are used, with each scatter symbol representing a mouse. n = 3 to 6 mice per group. Two-way ANOVA followed by Fisher's least significant difference (LSD) tests was conducted for statistical analysis. (**D**) Anatomical distribution of pathology scores derived from MC1 immunostaining in sham-treated (left) or rTBI-treated (right) 3-month-old PS19 mice preinoculated with synthetic tau PFFs. Average pathology scores were used for the heatmap.

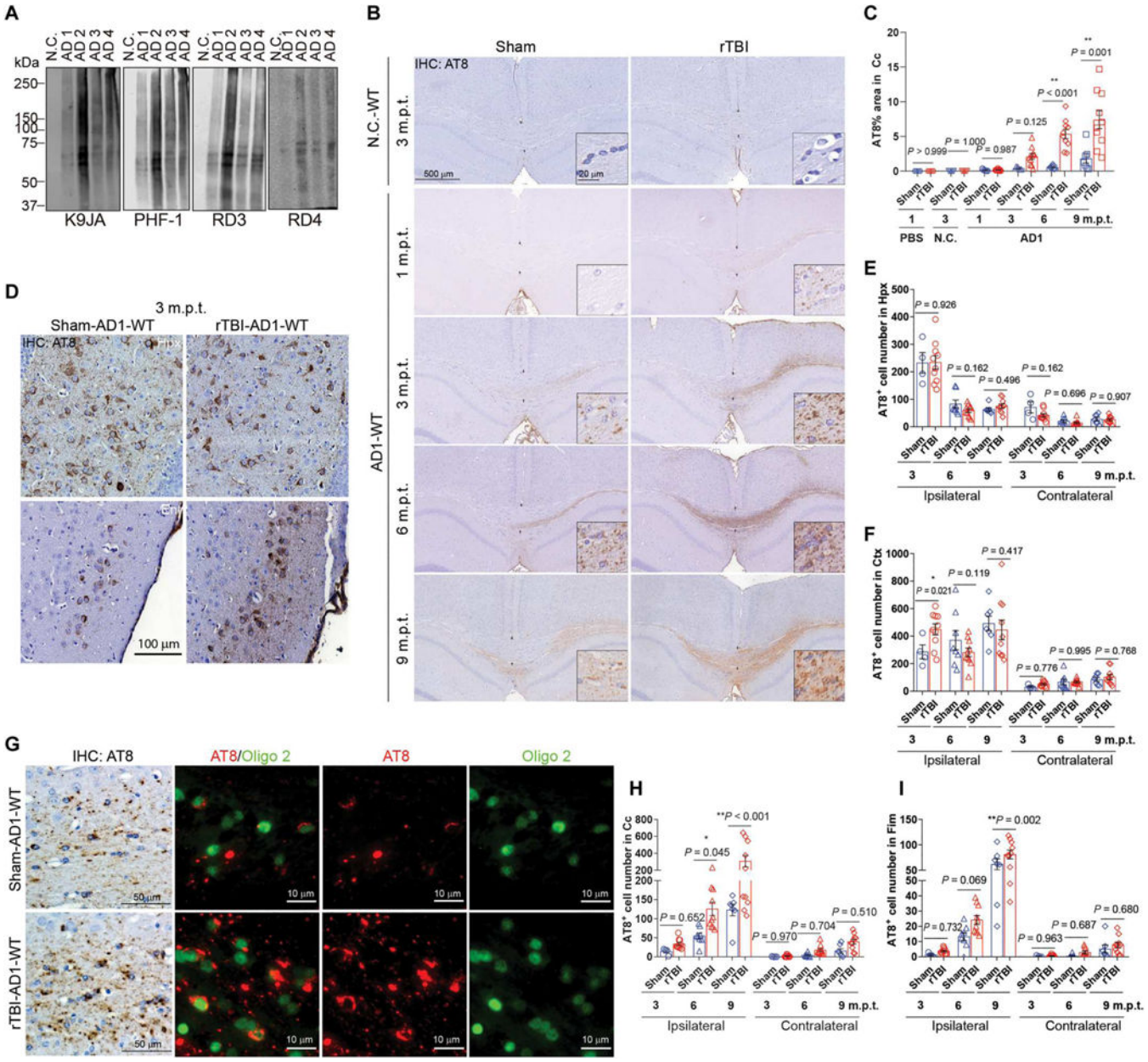

Fig. 5. rTBI accelerated tau pathogenesis in young WT mice preinoculated with human AD brain–derived pathological tau.

(**A**) Western blots of pathological tau extracted from 4 AD and 1 normal control (N.C.) cases, with antibodies: K9JA to pan-tau, PHF-1 to phosphorylated tau, RD3 to 3R (3-repeat) isoform–specific tau, and RD4 to 4R (4-repeat) isoform–specific tau. (**B**) Brain sections were stained by immunohistochemistry using the AT8 antibody to phosphorylated tau. Representative images of Cc of 3-month-old WT mice unilaterally inoculated with control lysate or human AD brain–derived pathological tau (AD1-tau) at different time points after sham (left) or rTBI (right) treatment are shown. Dashed white lines indicate the Cc area used for quantification. The black arrows indicate the regions for measuring the Cc thickness as shown in fig. S9B. Insets show higher magnification of Cc. (**C**) Quantification of AT8-

positive area in the Cc regions of the mice as shown in (B). (**D**) Brain sections were stained by immunohistochemistry using the AT8 antibody. Representative images of hippocampus (Hpx) and entorhinal cortex (Ent) of 3-month-old sham-treated (left) or rTBI-treated (right) WT mice unilaterally preinoculated with AD1-tau at 3 months post-treatment (m.p.t.) are shown. (**E** and **F**) Respective quantification of the AT8-positive NFT-like tau pathologies in the ipsilateral and contralateral sides of Hpx or cortices (Ctx) of 3-month-old sham-treated (left) or rTBI-treated (right) WT mice unilaterally preinoculated with AD1-tau at different time points after treatment. (**G**) Brain sections were stained by immunohistochemistry and immunofluorescence using the AT8 antibody and Oligo 2 antibody to oligodendrocyte nucleus. Representative images of Cc of 3-month-old sham-treated (top) or rTBI-treated (bottom) WT mice unilaterally inoculated with AD1-tau at 9 m.p.t. are shown. (**H**) Quantification of AT8-positive oligodendrocyte in the ipsilateral and contralateral sides of Cc of 3-month-old WT mice unilaterally inoculated with AD1-tau at different time points after rTBI or sham treatment (**I**) Quantification of AT8-positive oligodendrocytes in the fimbria (Fim) for the same treatment groups as in (H). $n = 4$ to 10 mice per group. Two-way ANOVA followed by Fisher's LSD tests was conducted for statistical analysis. Data are presented as means ± SEM, with each symbol representing a mouse.

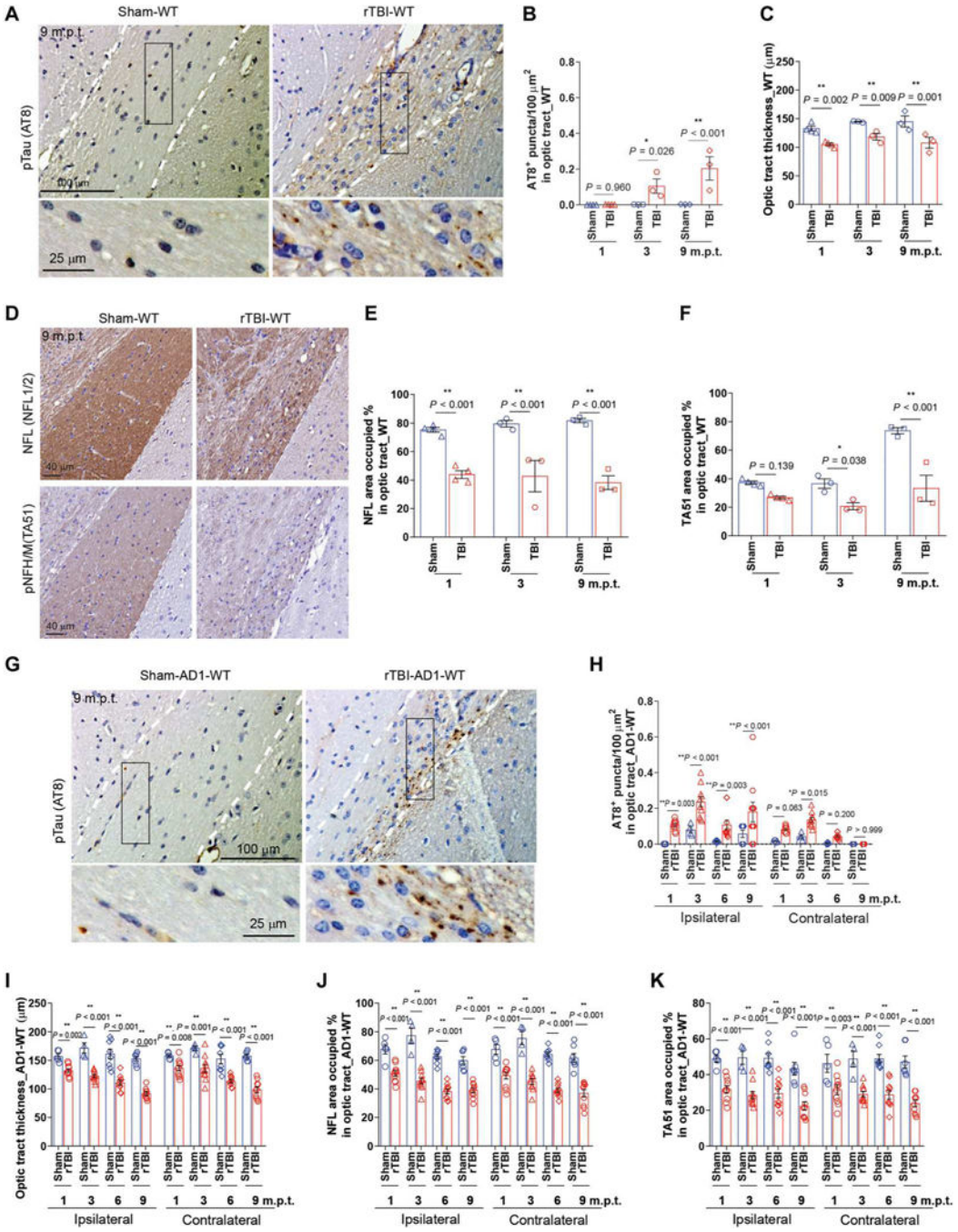

Fig. 6. rTBI alone induced punctate tau deposits in the optic tracts of WT mice.

(**A**) Sections were stained by immunohistochemistry using the AT8 antibody to phosphorylated tau. Representative images of optic tracts in 8-month-old sham-treated (left) or rTBI-treated (right) WT mice at 9 m.p.t. are shown. (**B**) Quantification of the AT8-positive tau puncta in the optic tracts of sham-treated (left) or rTBI-treated (right) WT mice at different time points after treatment. One-m.p.t. cohort mice started to receive the treatment at 3 months of age, whereas 3- and 9-m.p.t. cohort mice started to receive the treatment at 8 months of age. (**C**) Quantification of the optic tract thickness of the same mice

as shown in (B). (**D**) Sections were stained by immunohistochemistry using the NFL1/2 antibody to neurofilament light chain (NFL) or the TA51 antibody to phosphorylated neurofilament heavy and middle chain (pNFH/M). Representative images of the optic tracts in 8-month-old sham-treated (left) or rTBI-treated (right) WT mice at 9 m.p.t. are shown. (**E** and **F**) Respective quantification of NFL1/2- or TA51-positive axons in the optic tracts of the same mice as shown in (B). (**G**) Sections were stained by immunohistochemistry using the AT8 antibody. Representative images of the optic tracts in the 3-month-old sham-treated (left) or rTBI-treated (right) WT mice unilaterally preinoculated with human AD brain–derived pathological tau AD1-tau at 9 m.p.t. are shown. (**H**) Quantifications of AT8-positive tau puncta in the ipsilateral and contralateral optic tracts of the 3-month-old sham-treated (left) or rTBI-treated (right) WT mice unilaterally preinoculated with AD1-tau at different time points after treatment. (**I**) Quantification of the thickness of the ipsilateral and contralateral optic tracts of the same mice as shown in (H). (**J** and **K**) Quantifications of NFL1/2- or TA51-positive axons in the ipsilateral and contralateral optic tracts of the same mice as shown in (H). n = 3 to 10 mice per group. Scale bars are indicated in each image. Two-way ANOVA followed by Fisher's LSD tests were used to evaluate the rTBI effects. Data are presented as means ± SEM, with each symbol representing a mouse.

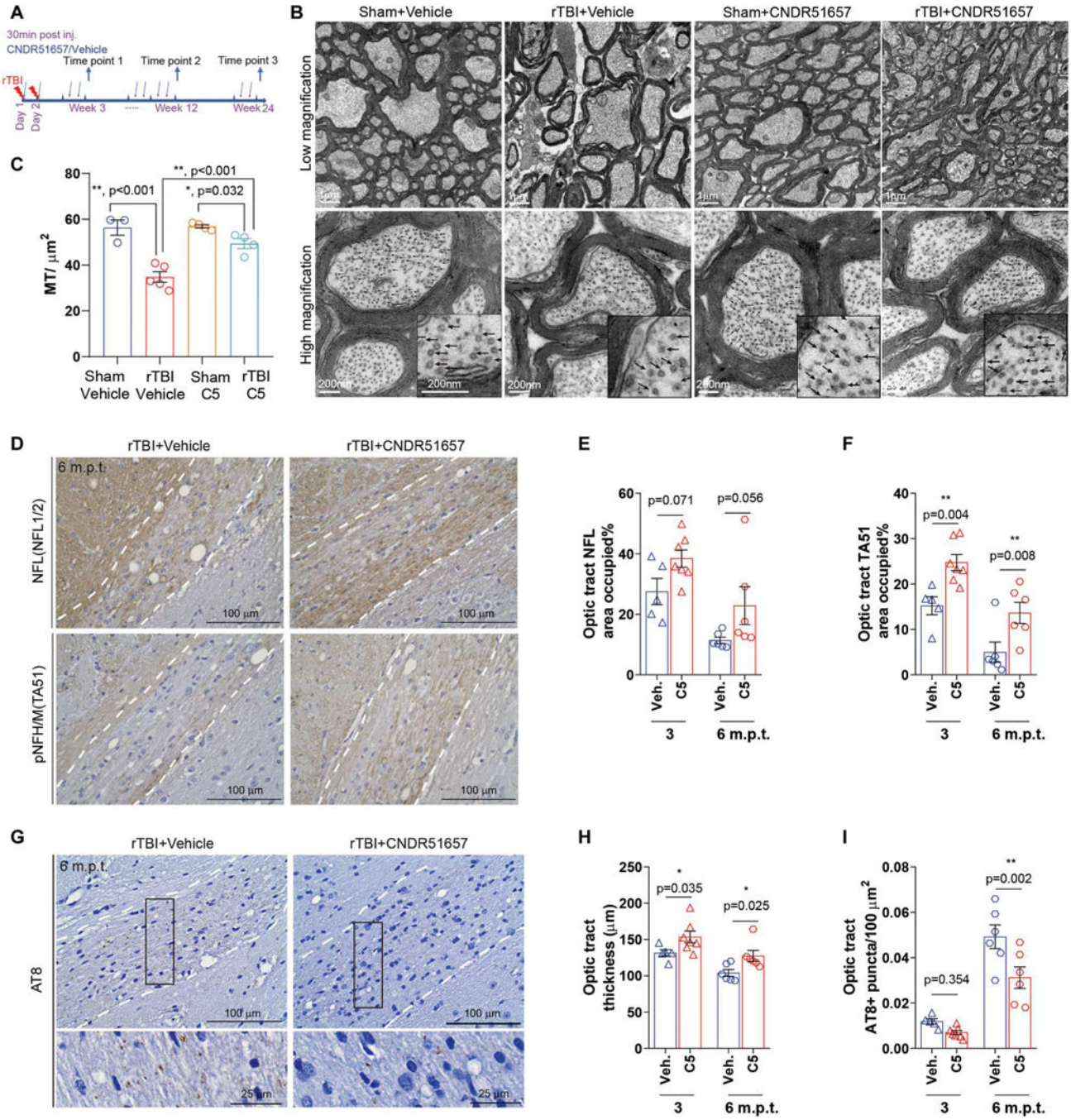

Fig. 7. Chronic CNDR51657 treatment alleviated microtubule disruption and tau accumulation in the optic tracts of rTBI-treated WT mice.

(**A**) Schematic of the experimental paradigm. CNDR51657 (3 mg/kg, intraperitoneally) or vehicle was administered after each rTBI session and then twice weekly for up to 24 weeks. Mice were sacrificed at three different time points. Note that the 3-w.p.t. and 3-m.p.t. mice were at 3 months of age, whereas the 6-m.p.t. mice were at 8 months of age, when receiving sham or rTBI treatment. (**B**) Representative transmission electron microscopy images of microtubules in the optic nerves of sham- or rTBI-treated WT mice 3 w.p.t.

Mice received either vehicle (Veh.) or CNDR51657 (C5) as indicated in (A). The ring-like structures indicated by black arrows in the higher-magnification images are microtubules. (**C**) Quantification of the microtubule density in the optic nerves as shown in (B). (**D**) Sections were stained by immunohistochemistry using the NFL1/2 antibody to NFL or the TA51 antibody to phosphorylated pNFH/M. Representative images of the optic tracts of WT mice at 6 m.p.t. along with the vehicle (left) or CNDR51657 (right) administration are shown. (**E** and **F**) Respective quantification of NFL- or TA51-positive axons in the optic tracts of mice that were administered either vehicle (left) or CNDR51657 (right) at 3 and 6 m.p.t. (**G**) Sections stained by immunohistochemistry using the AT8 antibody to phosphorylated tau. Representative images of optic tracts of WT mice at 6 m.p.t. along with the vehicle (left) and CNDR51657 (right) administration are shown. (**H**) Quantification of optic tract thickness at 3 and 6 m.p.t. (**I**) Quantification of AT8-positive puncta in the optic tracts of the mice at 3 and 6 m.p.t. $n = 3$ to 7 mice per group. Two-way ANOVA followed by Fisher's LSD multiple comparisons was conducted to analyze the effect of CNDR51657. Data are presented as means ± SEM, with each symbol representing a mouse. The representative images of 3 m.p.t. mice are shown in fig. S18 (A and B).

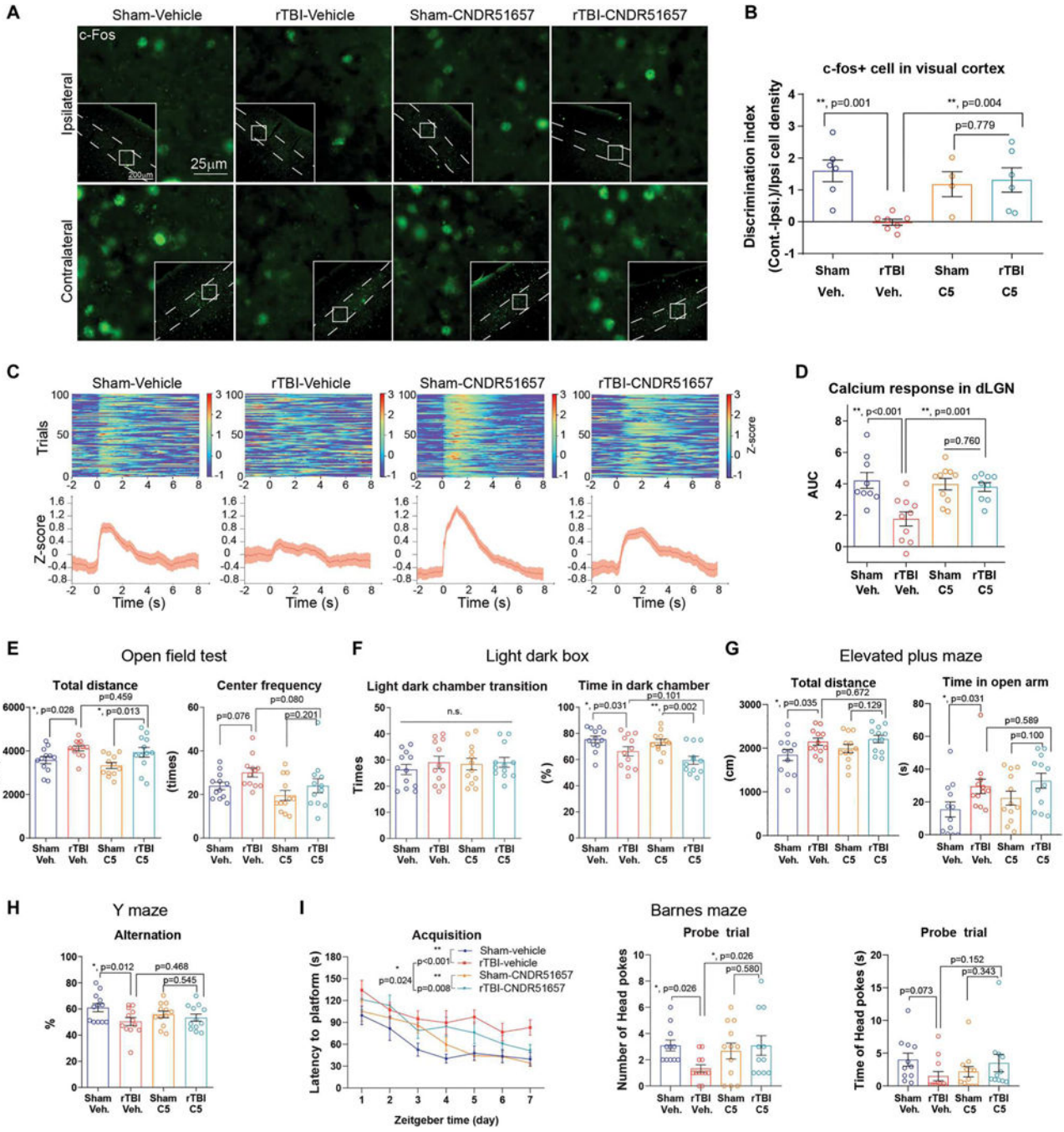

Fig. 8. Chronic CNDR51657 treatment improved visual and cognitive function in rTBI-treated WT mice.

(**A**) Sections containing the primary visual cortex (V1) were stained with a c-Fos antibody. Representative images of WT mice at 3 months after sham and rTBI treatment are shown. Animals were treated for 3 months with either vehicle (Veh.) or CDNR-51657 (C5). Insets show lower-magnification images of the V1 cortex. Dashed lines indicate V1 layer 4. (**B**) Differences in the number of c-Fos–positive neurons between ipsilateral and contralateral V1 are plotted as discrimination index. (**C**) (Top) Heatmaps of normalized calcium signals

recorded from the dLGN in response to light stimulation (at time 0). (Bottom) Ca^{2+} activity averaged across trials. (**D**) Quantification of the area under curve (AUC) of the Ca^{2+} signals after light stimulation (0 to 7 s) in dLGN as shown in (C). (**E**) Open field test was performed at 4 weeks after sham or rTBI treatments (w.p.t.). Mouse total distance (left) and the frequency to reach the central area (right) are presented. (**F**) Light-dark box test was performed at 4 w.p.t. The percentage of time spent in the dark chamber is summarized. (**G**) Elevated plus maze was performed at 9 w.p.t. The total distance traveled (left) and the total time spent in the open arm (right) are presented. (**H**) Y maze was performed at 10 w.p.t. The spontaneous alternations of arm exploration are plotted. (**I**) Barnes maze was performed at 12 w.p.t. The presented data show the latency to find the chamber platform during the acquisition phase (left), the number of head pokes (middle), and the time to find the target hole (right). $n = 4$ to 12 mice per group. Two-way or mixed-model ANOVA followed by Fisher's LSD tests was conducted for statistical analysis. Data are presented as means ± SEM, with each symbol representing a mouse. n.s., not significant.